Proteomic analysis to identify markers of exposure to cadmium sulphide quantum dots (CdS QDs)

Valentina Gallo
Universita degli Studi di Parma
Vaibhav Srivastava
KTH Royal Institute of Technology Gene technology
Vincent Bulone
KTH Royal Institute of Technology Gene technology
Andrea Zappettini
Istituto dei Materiali per l'Elettronica ed il Magnetismo Consiglio Nazionale delle Ricerche
Marco Villani
Istituto dei Materiali per l'Elettronica ed il Magnetismo Consiglio Nazionale delle Ricerche
Nelson Marmiroli
CINSA
Marta Marmiroli (marta.marmiroli@unipr.it)
Universita degli Studi di Cagliari Dipartimento di Scienze Chimiche e Geologiche

Research

Keywords: Baker's yeast, proteomics, iTRAQ, engineered nanomaterials, glycolysis, oxidative phosphorylation, endoplasmic reticulum

Posted Date: February 3rd, 2020

DOI: https://doi.org/10.21203/rs.2.22437/v1

Abstract

Background

The increasing use of cadmium sulphide (CdS) quantum dot (QD)-enabled products is expected to be accompanied by their release into the environment. In this study, the whole organism Saccharomyces cerevisiae was used as a model eukaryote to study protein modulations employing 2D- gel electrophoresis and gel-free iTRAQ (Isobaric Tags for Relative and Absolute Quantitation) proteomics following cell exposure to CdS QDs for 9 and 24 h. From both biotechnological and ecotoxicological perspectives, the use of *S. cerevisiae* as a model organism sheds light on the impact nanomaterials have on the biochemical responses of the exposed organism.

Results

Key proteins involved in essential biological pathways were downregulated, in particular after 24 h exposure. These include the major proteins of the glycolytic pathway, the components of mitochondrial respiratory chain complexes III, IV and V involved in the oxidative phosphorylation chain, the ATP-dependent molecular chaperone Hsc82 as well as other proteins responsible for protein folding and ubiquitination in the endoplasmic reticulum. Some of the proteins whose expression was altered have previously been described as strongly-adsorbed by CdS QD nanomaterial surfaces as hard corona, and involved in the cytotoxicity of this class of engineered nanomaterials. These data may be extrapolated to broader contexts and a wider range of organisms by allowing the identification of robust biomarkers of exposure to CdS QDs.

Conclusions

The work shows the power of the model organisms S. cerevisiae in biotechnology to ensure high levels of health and environmental safety. In fact, the double proteomic approach allowed to identify early markers of exposure to CdS QDs among all the proteins reprogrammed by the treatment.

Background

Engineered nanomaterials (ENMs) show novel and interesting physico-chemical properties that have stimulated their use in many products currently available on the market [(1)]. In the past decade, ENMs have become ubiquitous and a part of our daily life in the form of components of cosmetics, food packaging, drug delivery systems, therapeutics, electronic systems, biosensors, and many other daily products [(2)]. The value of the global nanocomposite market is predicted to reach $5.3 billion by 2021, with a compound annual growth rate of 26.7% [(3, 4)].

Among the numerous types of ENMs, quantum dots (QDs) are nanocrystals of semiconducting materials measuring around 2–10 nm, composed of metals belonging to groups II-V or III-V of the periodic table. They consist of a coated semiconductor inorganic core to improve optical and electronic properties [(5, 6)]. Owing to their narrow emission waveband, bright fluorescence tuneable according to their dimensions, high photo-stability and broad UV excitation, QDs were initially adopted in precision optical devices, [(7)] solar cells, [(8)] new generation LEDs and lasers [(9, 10)]. More applications of QDs include medical diagnostic tools and imaging

detection systems for biomarkers of cancer cells, [11, 12, 13] immunoassays, and cancer therapy, [14, 15] as well as transport vehicles for DNA, proteins and drugs to degenerative cells. [16-19]

As QD nanomaterials applications expand, the risk of exposure of the population and dispersal in the environment increases. Like all other ENMs, QDs have been investigated for their possible toxicity to human health and the environment. [20, 21] Initial studies attributed QDs toxicity mainly to the release of their Cd^{2+} ions. [22] However, this theory has been disproved [23, 24, 25] and the issue of QD toxicity mechanisms still remains to be clarified.

There are several reports of QD's toxic impact on human cell lines, simple eukaryotes, and plants, which correlate toxicity to the surface properties, size, and functionalization of the nanomaterials. [25, 28, 29] It has been found that CdS QDs cause complete reprogramming of the transcriptome of *Saccharomyces cerevisiae* and *Arabidopsis thaliana,* alteration of reactive oxygen species (ROS) production in human cells, readjustment in oxidative stress responses (enzymatic and non-enzymatic) and damage to mitochondrial functionality. [23, 25, 29] Paesano *et al*. (2016) reported that CdS QDs trigger apoptosis, increase ROS concentrations, and modify the transcription of key genes in HepG2 liver cells. [26] Similar results have been reported by Zhang *et al.,* (2016) upon *in vivo* and *in vitro* exposure to CdTe QDs of mice liver cells, [30] and by Fan *et al.,* (2016) when exposing HL-7702, HepG2, HEK-293 cell lines to CdTe/CdS core/shell QDs. [31]

There is need of a paradigm shift in nanotoxicology, as advocated by the US National Academies of Sciences (2007). Also, EU legislation promotes Intelligent or Integrated Testing Strategies (ITS) for chemicals and specifically for ENMs (REACH Directive 1907/2006). In general, toxicology regulations for the 21st century promote the use of more efficient and more ethical tests, and encourage identification of toxicity mechanisms to build evidence-based testing strategies, and promote the use of *in vitro*, high-throughput screening (HTS) using cell lines and model organisms such as *S. cerevisiae* which has 20% homology with the human genome. [32] Among the key elements in this new approach to toxicology is the widely accepted 3Rs (Reach) principle, which aims to replace, reduce, and refine animal testing. [33].

To explore the mechanism of ENMs toxicity, new *in vitro* and *in silico* approaches together with the application of HTS have been advocated. [20] In particular, "omics"-based platforms applied to model organisms have provided key information on the interaction between ENMs and living material. [25 34,35]

S. cerevisiae is a unicellular eukaryote and one of the most-used model organisms for molecular biology. [36] The proteome of *S. cerevisiae* was one of the first to be elucidated. [37] Its genome of about 12 Mb is distributed in 16 chromosomes and has been completely sequenced and annotated. [38] The ease of use of this yeast, its rapid life cycle (about 2 h at 28°C) and the availability of several molecular and genomic tools, make it an excellent platform for toxicological studies. [32] Furthermore, the high level of functional conservation across the genomes of other eukaryotes, including humans, makes yeast a model system to assess the mechanisms of response to a wide range of molecules and ENMs. [39, 29, 40] Indeed, *S. cerevisiae* represents an ideal experimental system from a genome-wide perspective to study mechanisms through the combination of quantitative transcriptomics and proteomics. [41] Proteomic methods allow the global analysis of gene products in various physiological states of cells and yeasts can readily be analysed using

proteomic tools. [37] Protein profiles provide a map of the biochemical status of stressed cells and organisms closely related to overall phenotypic responses. [42, 43]

In this work, a comparative proteomics analysis was employed to dissect the mechanisms of toxicity of CdS QDs in *S. cerevisiae*. We have investigated the most significant responses of this yeast to sub-lethal concentrations of CdS QDs at two time points, 9 and 24 h, by using 2D-gel electrophoresis followed by MALDI TOF MS-MS as well as the quantitative iTRAQ proteomics approach followed by LC-MS. Comparative proteomics utilizing gel-based and gel-free approaches has already been successfully applied to *S. cerevisiae.* [44-46] Our aim was to identify the proteomic alterations underlying the cell response to CdS QDs. The data facilitate understanding the detrimental effects that these ENMs have on the environment and human health.

Results And Discussion

Cell growth in the different conditions tested

S. cerevisiae strain BY4742 was grown on either YPD or SD medium with CdS QD concentrations of 25 to 200 mg L^{-1}. The colony spot assay showed that yeast cells grew better on YPD than on SD medium, therefore YPD was chosen for all subsequent experiments (Fig. 1A). When nystatin was added at 0.25 mg L^{-1} [29] growth curve assays comparable to the control in YPD were obtained in the presence of 100 mg L^{-1} of CdS QDs (Fig. 1B). The concentration of 100 mg L^{-1} CdS QDs, with and without 0.25 mg L^{-1} nystatin, was chosen as the treatment for subsequent analyses. [25, 29] The growth and treatment selected were identical to those used in previous transcriptomics analyses, [25, 28] allowing comparison between affected transcripts and proteins upon treatment with CdS QDs. Duration of the treatment was first set at 9 h, which corresponds to the exponential growth phase of the yeast cultures, and then at 24 h for the stationary phase. Cell cultures sampled at the exponential phase showed an OD_{600} value of about 2.5 for the control and 0.6 for QDs treatment, whereas cultures harvested at the stationary phase showed an OD_{600} value of about 12.0 for the control and 4.5 for QDs treatment with and without nystatin.

Proteomic variations in response to CdS QDs

Qualitative and quantitative changes in the yeast proteome during CdS QDs treatments were obtained from the 2D-PAGE-based and gel-free iTRAQ approaches, respectively. [45, 46] Common proteins identified with the two methods and after the two times of treatments are represented in Figs. 2 and 3 and in Table 1.

Table 1
List of the differentially expressed proteins after 9 h treatment 2D-gel (A), iTRAQ (B), and 24 h treatment (iTRAQ) (C).

	Proteins	Gene	pathway code	pathway name	description
B C	3-isopropylmalate dehydratase	LEU1	sce00290 sce01100 sce01110 sce01230	Valine leucine and isoleucine biosynthesis Metabolic pathway Biosynthesis of secondary metabolites Biosynthesis of amino acids	Catalyzes the isomerization between 2-isopropylmalate and 3-isopropylmalate, via the formation of 2-isopropylmaleate.
B C	78 kDa glucose-regulated protein homolog	KAR2	sce03060 sce04141	Protein export Protein processing in endoplasmic reticulum	Probably plays a role in facilitating the assembly of multimeric protein complexes inside the ER. Is required for secretory polypeptide translocation.
B C	Adenylosuccinate lyase	ADE13	sce00230 sce00250 sce01100 sce01110 sce01130	Purine metabolism Alanine, aspartate and glutamate metabolism Metabolism secondary Biosynthesis of secondary metabolites Biosynthesis of antibiotics	This protein is involved in the subpathway that synthesizes AMP from IMP.

	Proteins	Gene	pathway code	pathway name	description
A B C	ATP-dependent molecular chaperone HSC82	HSC82	sce04141	Protein processing in endoplasmic reticulum	Molecular chaperone that promotes the maturation, structural maintenance and proper regulation of specific target proteins involved in cell cycle control and signal transduction. Undergoes a functional cycle that is linked to its ATPase activity. Interacts dynamically with various co-chaperones that modulate its substrate recognition, ATPase cycle and chaperone function.
B C	Bifunctional purine biosynthesis protein ADE17	ADE17	sce00230 sce00670 sce01110 sce01130	Purine metabolism One carbon pool by folate Secondary metabolites Biosynthesis of antibiotics	This protein is involved in the subpathway that synthesizes 5-formamido-1-(5-phospho-D-ribosyl)imidazole-4-carboxamide from 5-amino-1-(5-phospho-D-ribosyl)imidazole-4-carboxamide (10-formyl THF route).
A C	Carnitine O-acetyltransferase, mitochondrial	CAT2	sce04146	Peroxisome	Carnitine acetylase is specific for short chain fatty acids. It seems to affect the flux through the pyruvate dehydrogenase complex. It may be involved as well in the transport of acetyl-CoA into mitochondria.

	Proteins	Gene	pathway code	pathway name	description
B C	Cystathionine gamma-lyase	CYS3	sce00260 sce00270 sce00450 sce01100 sce01130 sce01230	Glycine sereine and threonine metabolism Cysteine and methionine metabolism Seleno compound metabolism Metabolic pathway Biosynthesis of antibiotics Biosynthesis of amino acid	This protein is involved in the subpathway that synthesizes L-cysteine from L-homocysteine and L-serine.
B C	Elongation factor 1-beta	EFB1			Catalytic subunit of the guanine nucleotide exchange factor (GEF) (eEF1B subcomplex) of the eukaryotic elongation factor 1 complex (eEF1).
A C	Enolase 1	ENO1	sce00010 sce00680 sce01100 sce01110 sce01130 sce01200 sce01230 sce03018	Glycolysis / Gluconeogenesis Methane metabolism Metabolic pathway Biosynthesis of secondary metabolites Biosynthesis of antibiotics Carbon metabolism Biosynthesis of amino acid RNA degradation	This protein is involved in the subpathway that synthesizes pyruvate from D-glyceraldehyde 3-phosphate.
B C	FACT complex subunit POB3	POB3			Component of the FACT complex, a general chromatin factor that acts to reorganize nucleosomes.
B C	Flavohemoprotein	YHB1			Is involved in NO detoxification in an aerobic process.

	Proteins	Gene	pathway code	pathway name	description
A B C	Fructose-bisphosphate aldolase	FBA1	sce00010 sce00030 sce00051 sce00680 sce01100 sce01110 sce01130 sce01200 sce01230	Glycolysis / Gluconeogenesis pentose phosphate pathway fructose and mannose metabolism methane metabolism metabolic pathway biosynthesis of secondary metabolites biosynthesis of antibiotics carbon metabolism biosynthesis of amino acid	Catalyzes the aldol condensation of dihydroxyacetone phosphate (DHAP or glycerone-phosphate) with glyceraldehyde 3-phosphate (G3P) to form fructose 1,6-bisphosphate (FBP) in gluconeogenesis and the reverse reaction in glycolysis.
B C	Glutamate synthase [NADH]	GLT1	sce00250 sce00910 sce01100 sce01110 sce01130 sce01230	Alanine aspartate glutamate metabolism Nitrogen metabolism Metabolic pathway Secondary metabolites Biosynthesis of antibiotics Biosynthesis of amino acid	Forms L-glutamate from L-glutamine and 2-oxoglutarate
B C	Glutamine synthetase	GLN1	sce00250 sce00220 sce00630 sce00910 sce01100 sce01230	Alanine aspartate glutamate metabolism Arginine biosynthesis Glyoxylate and dicarboxylate metabolism Nitrogen pathway Metabolic pathway Biosynthesis of amino acid	ATP binding and glutamate-ammonia ligase activity
B C	Heat shock protein 26	HSP26	sce04141	Protein processing in endoplasmic reticulum	One of the major polypeptides produced on heat shock.

	Proteins	Gene	pathway code	pathway name	description
B C	Heat shock protein SSA1	SSA1	sce04140 sce04141 sce04144 sce04213	Spliceosome Protein processing in endoplasmic reticulum Endocytosis Longevity regulating pathway	May play a role in the transport of polypeptides both across the mitochondrial membranes and into the endoplasmic reticulum.
A B C	Homocysteine/cysteine synthase	MET17	sce00270 sce00920 sce01100 sce01110 sce01130 sce01200 sce01230	Cysteine and methionine metabolism Sulphur metabolism Metabolic pathway Biosynthesis of secondary metabolites Biosynthesis of antibiotics Carbon metabolism Biosynthesis of amino acid	Catalyzes the conversion of O-acetyl-L-homoserine (OAH) into homocysteine in the methionine biosynthesis pathway.
B C	NADPH-dependent alpha-keto amide reductase	YDL124W			Involved in mitochondrial protection of cadmium-induced oxidative stress.
B C	NAD-specific glutamate dehydrogenase	GDH2	sce00220 sce00250 sce00910 sce01100	Arginine biosynthesis Arginine alanine glutamine biosynthesis Nitrogen metabolism Metabolic pathway	NAD^+-dependent glutamate dehydrogenase which degrades glutamate to ammonia and alpha-ketoglutarate.
B C	Peptidyl-prolyl cis-trans isomerase D	CPR5			Plases accelerate the folding of proteins. It catalyzes the cis-trans isomerization of proline imidic peptide bonds in oligopeptides.

	Proteins	Gene	pathway code	pathway name	description
B C	Peroxiredoxin TSA1	TSA1			Thiol-specific peroxidase that catalyzes the reduction of hydrogen peroxide and organic hydroperoxides to water and alcohols, respectively.
B C	Potassium-activated aldehyde dehydrogenase, mitochondrial	ALD4	sce00010 sce00071 sce00280 sce00310 sce00620 sce01110	Glycolysis / Gluconeogenesis Fatty acid degradation Valine leucine isoleucine degradation Lysine degradation Pyruvate metabolism Metabolic pathway	Potassium-activated aldehyde dehydrogenase involved in acetate formation during anaerobic growth on glucose.
A C	Protein HBT1				Polarity-determining protein which forms a conjugate with the ubiquitin-like modifier HUB1. Involved in bud site selection and cellular morphogenesis during conjugation.
B C	Ribosomal protein L15	K7_RPL15A			structural constituent of ribosome
B C	S-adenosylmethionine synthase 2	SAM2	sce00270 sce01100 sce01110 sce01230	Cysteine and methionine metabolism Metabolic pathway Secondary metabolites Amino acid biosynthesis	Catalyzes the formation of S-adenosylmethionine from methionine and ATP.

	Proteins	Gene	pathway code	pathway name	description
B C	Serine hydroxymethyltransferase, cytosolic	SHM2	sce00260 sce00460 sce00630 sce00670 sce00680 sce01100 sce01110 sce01130 sce01200 sce01230	Glycine serine and threonine metabolism Cyanoamino acid metabolism Glyoxylate and dicarboxylate metabolism One carbon pool by folate Methane metabolism Metabolic pathways Biosynthesis of secondary metabolites Biosynthesis of antibiotics Carbon metabolism Biosynthesis of amino acids	Interconversion of serine and glycine.
B C	Succinate dehydrogenase [ubiquinone] flavoprotein subunit, mitochondrial	SDH1	sce00020 sce00190 sce01100 sce01110 sce01130 sce01200	Citrate cycle Oxidative phosphorylation Metabolic pathway Biosynthesis of secondary metabolites Biosynthesis of antibiotics Carbon metabolism	Catalytic subunit of succinate dehydrogenase (SDH) that is involved in complex II of the mitochondrial electron transport chain and is responsible for transferring electrons from succinate to ubiquinone (coenzyme Q).
B C	Sulfite reductase [NADPH] subunit beta	MET5	sce00920	Sulfur metabolism	Catalyzes the reduction of sulfite to sulfide, one of several activities required for the biosynthesis of L-cysteine from sulfate.
B C	UBX domain-containing protein 1	SHP1	sce04101	Protein processing in endoplasmic reticulum	Involved in CDC48-dependent protein degradation through the ubiquitin/proteasome pathway.

	Proteins	Gene	pathway code	pathway name	description
A B C	Uncharacterized oxidoreductase YMR226C	YMR226C	sce00240 sce00260 sce01100	Pyrimidine metabolism Glycine serine threonine biosynthesis Metabolic pathway	NADP-dependent dehydrogenase with broad substrate specificity acting on 3-hydroxy acids.
B C	Uracil phosphoribosyltransferase	FUR1	sce00240 sce01100	Pyrimidine metabolism, Metabolic pathway	Catalyzes the conversion of uracil and 5-phospho-alpha-D-ribose 1-diphosphate (PRPP) to UMP and diphosphate.

Identification of differentially expressed proteins with 2D-PAGE

For the yeast cells exposed to CdS QDs for 9 h, with and without nystatin, the 2D-PAGE approach allowed the visualisation of around 900 spots for each sample. Subsequent MALDI-TOF MS-MS analysis allowed the identification of about 270 spots (Figure S3). Within the former group, 100 spots varied in intensity in response to the treatments: 81 of these differed from the control (ctr, not treated) vs QDs; 78 were different between ctr and nystatin + QDs; 11 differed between ctr and nystatin; and 72 differed between the nystatin and nystatin + QDs samples.

The CdS QDs treatment, with and without nystatin, altered the expression level of 56 common proteins as found by comparing ctr and QDs; ctr and nystatin + QDs; and nystatin vs nystatin + QDs. Among the 11 proteins affected by the treatment with nystatin, only 4 were common to other treatments, and were thus identified, whilst those proteins that were present exclusively in the samples treated with nystatin were excluded from the analysis of the effect of CdS QDs (Fig. 2A). At 9 h, there is a balance in the number of the modulated proteins between up and downregulated (fig S7A). The identities of the protein spots, whose abundance was differentially modulated with a p value of ≤ 0.05 is presented in Table S1.

Identification of the differentially expressed proteins using iTRAQ labelling

The time points for quantitative iTRAQ analysis were 9 and 24 h. This gel-free approach allowed processing more samples than 2D-PAGE, therefore proteome variations were also analysed under all treatments and both time points. The iTRAQ approach enables quantification at the peptide level and direct protein mapping because both types of information originate from the same MS-MS spectra. In several other iTRAQ studies, about a thousand proteins were identified. [47 48] Far more than a thousand proteins were detected here within each single iTRAQ experiment on each biological replicate (Figure S4 and S5).

The iTRAQ experiments corresponding to 9 h of treatment allowed the identification and quantification of 1129 (934 quantified), and 1055 (835) unique proteins from the two biological replicates BR1 and BR2, respectively (Figure S4 and Supplementary Table S2). Of these, 849 (712) proteins were common to both biological replicates.

The iTRAQ analysis revealed 92 proteins enriched in the yeast cells in response to the treatments with CdS QDs, with and without nystatin: 62 of these proteins were identified by comparing ctr vs QDs; 45 were identified from the comparison of ctr and nystatin + QDs, 16 by comparing ctr vs nystatin and 59 by comparing the nystatin and nystatin + QDs samples. The CdS QD treatment altered the abundance level of 71 common proteins between ctr vs QDs, ctr vs nystatin + QDs and nystatin vs nystatin + QDs. Only 4 proteins from the comparison of ctr vs nystatin were identified because the other 10 proteins were not in common with any other treatment and therefore were not considered relevant. (Fig. 2B). Nevertheless, at 9 h the iTRAQ results complement the 2D-PAGE results by reconfirming the general trends and supporting the identification of specific protein clusters affected by CdS QD exposure (Figure S7B). The complementary nature of these methods was highly useful: proteins identified with 2D-PAGE and iTRAQ differ substantially as shown in Figure S6 and in Table 4, but the combined use of different techniques uncovers a higher proportion of the proteome of an organism. [(49)] The list of proteins identified in the two biological replicates and the proteins common to all samples are shown in Tables S2 and S4.

The iTRAQ analysis of the 24 h samples allowed the identification of 943 (886 quantified), and 1346 (1080) unique proteins from the two biological replicates BR1 and BR2, respectively (Figure S5 and Supplementary Table S3). Of these, 562 (505) proteins were common to the two biological replicates.

The iTRAQ-based quantitative analysis revealed that the total number of proteins enriched in the yeast cells in response to all treatments with CdS QDs, with and without nystatin, was 127. Eighty- eight of these proteins were identified by comparing ctr vs QDs, 86 by comparing ctr and nystatin + QDs, 23 by comparing ctr vs nystatin and 94 from the difference between the nystatin and nystatin + QDs samples. The CdS QD treatment altered the expression level of 59 common proteins as judged from the comparison of ctr vs QDs, ctr vs nystatin + QDs, and nystatin vs nystatin + QDs. Only 15 proteins were identified from the comparison between ctr vs nystatin because the other 8 proteins were not common to the other treatments and were therefore not considered relevant (Fig. 2C and S7C). The lists of proteins identified in two biological replicates and proteins common to all datasets are shown in Tables S3 and S4. Notably, at 24 h the modulated proteins showed a different trend to the finding after 9 h of treatment, i.e. the majority of the proteins were downregulated (Figure S7C).

We pooled together all the proteins identified for the 9 h treatments obtained with both methods, and compared them with those obtained for the 24 h treatment resulting from the iTRAQ method. Four proteins were in common between the two methods at both 9 h and 24 h: ATP-dependent molecular chaperone Hsp82, uncharacterised oxidoreductase YMR226C, fructose-bisphosphate aldolase (Fba1), and homocysteine/cysteine synthase (Met17) (Fig. 3 and Table S4). However, another 4 proteins were in common between the 2D -gel method at 9 h and iTRAQ at 24 h. These proteins were: carnitine O-acetyltransferase mitochondrial (Cat2), folic acid synthesis protein (Fol1), serine/threonine-protein kinase Ypk1, and succinate dehydrogenase [ubiquinone] iron-sulphur subunit (Sdh2). Another 26 proteins were in common between the

iTRAQ method at 9 h and iTRAQ at 24 h. The most downregulated proteins were elongation factor 1-beta (Efb1) and glutamate synthase (Glt1), and the most upregulated proteins were S-adenosylmethionine synthase 2 (Sam2) and superoxide dismutase 1 copper chaperone (Ccs1) (Fig. 3, Table 1 and Table S4).

Ontology analysis of the identified proteins

Analysis using gene ontology (GO) groups proteins based on biological processes, molecular functions, and cellular components. A GO term difference with a $p < 0.05$ was considered as significant enrichment. This annotation of proteins into different classes was instrumental to understanding their biological relevance. Functional in silico classification of the 192 proteins obtained at 9 h with both 2D-PAGE and iTRAQ labelling and the 119 proteins identified with iTRAQ at 24 h, was achieved via GO analysis using the software PANTHER. A total of 39 slim GO terms were significantly enriched ($p < 0.05$). PANTHER grouped all the enriched proteins at 9 h into four groups based on their molecular functions (Figure S8A): small molecule binding (4.88%), oxidoreductase activity (3.95%), structural constituent of ribosome (3.17%) and catalytic activity (1.75%). The major molecular GO functions for the 24 h samples were: oxidoreductase activity (6.03%), proton transmembrane transporter activity (5.02%), and catalytic activity (2.10%) (Figure S8B).

When the enriched proteins identified at 9 h were analysed on the basis of biological processes, they were organized in five major groups: organic acid biosynthetic process (4.82%), carboxylic acid biosynthetic process (4.82%), carbohydrate metabolic process (4.69%), primary metabolic process (3.47%), and metabolic process (1.70%). The enriched proteins obtained for the 24 h treatment were subdivided in 15 groups, of which the more important were: aerobic respiration (15.63%), tricarboxylic acid cycle (15.05%), cellular respiration (13.04%), energy derivation by oxidation of organic compounds (13.04%), oxidation-reduction process (10.67%), ATP synthesis coupled proton transport (9.23%), energy coupled proton transport (9.23%), and carbohydrate metabolic process (5.28%) (Fig. 4A and B). The main GO cell component categories for the 9 h treatment were: cytosolic ribosome (3.45%) and cytosolic part (3.15%). The samples recovered after 24 h treatment were enriched in mitochondrial inner membrane (5.08%) and cytoplasmic (1.61%) proteins (Figure S8C and S8D).

GO analysis of the differentially abundant proteins identified ‘oxidoreductase activity’ and ‘catalytic activity’ as the most perturbed biochemical functions in response to CdS QD exposure at 9 and 24 h, whilst the GO biological processes that differ between the two times of exposure corresponded to ‘carbohydrate metabolic process’ and ‘metabolic process’. Analysis of the significant biological processes affected at 24 h revealed that the majority of the GO classes were downregulated, in particular aerobic respiration, tricarboxylic acid cycle, cellular respiration, energy derivation by oxidation of organic compounds, oxidation-reduction process, and ATP synthesis coupled proton transport. Overall these results show that the treatment with CdS QDs is time-dependent.

In particular, two of the downregulated proteins that belong to each of the aerobic respiration, cellular respiration and tricarboxylic acid (TCA) cycle classes were citrate synthases CIT1 and CIT2. In eukaryotes, the TCA cycle occurs in the mitochondrial matrix and plays a pivotal role in the utilization of non-fermentable carbon sources via oxidative generation of reducing equivalents (NADH), driving aerobic respiration to yield ATP. [(50)] The TCA cycle is also an important source of biosynthetic building blocks, such as α-ketoglutarate,

succinyl-CoA and oxaloacetate, which are required for the synthesis of glucose and amino acids. [50] Yeasts have multiple citrate synthase genes (CIT1, CIT2, and CIT3), but it is not clear how they differ in function or if any of them encode a specific methylcitrate synthase. The products of the CIT1 and CIT3 genes have been shown to be mitochondrial proteins, whereas that of the CIT2 gene is clearly peroxisomal. [51]

The foregoing molecular function and biological processes mostly linked to mitochondrial function and structure represent the “core response” to CdS QDs. These data are in keeping with other results obtained from simple eukaryotic organisms and human cell lines. [25, 28, 26] From a physiological and molecular point of view, it has been demonstrated that ENMs increase ROS production by interacting negatively with all cell compartments, in particular by affecting cell membranes and the mitochondria and, consequently, the levels of energy production and cellular respiration. [25] The correspondence between ROS production and inhibition of respiration has been reported in the literature. For example, Fe_3O_4 nanoparticles have an inhibitory effect on yeast growth. The inhibition is attributed to their interaction with the mitochondria, leading to disruption of the mitochondrial respiratory chain complex IV, and consequent attenuation of ATP production. [52] In addition, it has been found that NiO NPs inhibit metabolic activity, induce intracellular accumulation of ROS, and provoke cell death in S. cerevisiae. [53]

Pathway analysis of the identified proteins

Metabolic pathway analysis was performed by submitting the Gene IDs of the proteins to the KEGG server (http://www.kegg.jp) for S. cerevisiae to identify the pathways that were represented more frequently. At 9 h the main pathway classes were: general metabolic pathway, biosynthesis of secondary metabolites, biosynthesis of amino acids, glycolysis and gluconeogenesis, protein biosynthesis, carbon metabolism, and protein processing in endoplasmic reticulum (ER) (Fig. 5).

At 24 h the main pathway classes were: general metabolic pathway, biosynthesis of secondary metabolites, oxidative phosphorylation, TCA cycle, glycolysis and gluconeogenesis, pyruvate metabolism, protein biosynthesis, carbon metabolism, and protein processing in endoplasmic reticulum (ER) (Fig. 5).

Of particular interest was the pathway “glycolysis and gluconeogenesis”, common to the two treatment times (Fig. 6), which included 13 proteins identified at 9 h, and 11 at 24 h. At 9 h of treatment, eight enzymes associated to the glycolysis pathway were over-abundant: NADP-dependent alcohol dehydrogenase 6 (Adh6), NADP-dependent alcohol dehydrogenase 7 (Adh7), glyceraldehyde-3-phosphate dehydrogenase 1 (Tdh1), glyceraldehyde-3-phosphate dehydrogenase 3 (Tdh3), glucose-6-phosphate isomerase (Pgi1), glucokinase-1 (Glk1), mitochondrial pyruvate dehydrogenase complex protein X component (Pdx1), and mitochondrial potassium-activated aldehyde dehydrogenase (Ald4). Five enzymes were under-abundant: fructose-bisphosphate aldolase (Fba1), enolase 1 (Eno1), enolase 2 (Eno2), pyruvate decarboxylase isozyme 1 (Pdc1), pyruvate decarboxylase isozyme 1(Pfk2).

At 24 h of treatment, the majority of the enzymes associated the glycolytic pathway were under-abundant: fructose-1,6-bisphosphatase (Fbp1), fructose-bisphosphate aldolase (Fba1), enolase 1 (Eno1), acetyl-coenzyme A synthetase 1 (Acs1), dihydrolipoyl dehydrogenase (Ldp1), mitochondrial dihydrolipoyl dehydrogenase (Ldp1), pyruvate decarboxylase isozyme 5 (Pdc5), mitochondrial potassium-activated

aldehyde dehydrogenase (Ald4), and NADP-dependent alcohol dehydrogenase 2 (Adh2). Only two enzymes were detected at levels higher than the control: hexokinase-1 (Hxk1) and glyceraldehyde-3-phosphate dehydrogenase 2 (Tdh2).

Among the enzymes common between 9 h and 24 h, Fba1 and Eno1 were under-abundant at both times of treatment, whereas the levels of Ald4 were initially increased at 9 h, then decreased at 24 h. As reported by Gomes et al. (2006) ENMs treatment inhibited the glycolytic pathway and stimulated fermentation. [54] Horstmann et al., (2019) suggested as highly probable that sugar transport genes and sugar-utilising enzyme genes are simultaneously affected by the presence of Cd-QDs. [55] They conjecture that the ENO1 gene is downregulated as a consequence of transport of low levels of sugars caused by the suboptimal activity of glucose transporters due to the presence of Cd-QDs. Conversely, the three isoforms of glyceraldehyde-3-phosphate dehydrogenase, GAPDH (Tdh1, Tdh2, Tdh3), were found to be upregulated for both treatment times. GAPDH is a glycolytic enzyme involved in glucose degradation and energy yield. It catalyses the sixth step of glycolysis, i.e. the conversion of glyceraldehyde-3-phosphate to 1,3 bis-phosphoglycerate, but also displays non-glycolytic activity in certain subcellular locations. In vitro inhibition studies of GAPDH in the presence of QDs suggest that binding of QDs to the enzyme molecules slows down the rate of the reactions catalysed by the enzyme, suggesting that QDs may act as enzyme inhibitors. [56] When human cancer cells are exposed to QDs, the loss of cellular GAPDH activity causes a metabolic perturbation during glycolysis, and the inhibition of GAPDH leads to the decrease of glycolytic rates. This suggests a possible mechanism of change in energy production from the glycolytic pathway to fermentation during QD-mediated cellular injury. This process may lead eventually to cell dysfunction and death. [56]

Proteins leading to the Krebs cycle (Pdx1, Acs1, Lpd1, Ald4) or to fermentation (Adh2, Adh6, Adh7, Pdc1, Pdc5) were modulated during treatment with CdS QDs for both periods (Table S4 and Fig. 6). Pdc1 is the most prevalent form of the three yeast pyruvate decarboxylases which are involved both in the anaerobic fermentation of pyruvate to acetaldehyde and in amino acid catabolism. Pdc1, together with Tdh2 and Tdh3, was found among the proteins that constitute the hard corona in yeast during CdS QDs treatments, with a specific role in determining the toxicity of these ENMs. [57]

Another pathway of particular interest is “protein processing in ER”, which includes 7 proteins modulated at 9 h (2 under-abundant and 5 over-abundant) and 6 at 24 h (2 proteins with reduced levels and 3 with increased levels) (Fig. 7). Three common enzymes were found to be overexpressed at the two times of treatments: ATP-dependent molecular chaperone Hsc82, 78 kDa glucose-regulated protein homolog (Kar2) and UBX domain-containing protein 1 (Shp1). Hsc82, a member of the Hsp90 family, acts to promote the maturation, structural maintenance and regulation of proteins involved in cell cycle control, ribosome stability and signal transduction. [58] Hsp90 proteins operate in a number of signalling pathways which are altered during exposure to metal ENMs. [59] It was shown that Hsc82 is one of the main hubs in CdS QDs sensitivity, [28] and that it is one of the hard corona proteins for CdS QDs. [57]

Other two enzymes of the ER were present at higher levels at 9 h and lower levels at 24 h. These enzymes were heat shock protein 26 (Hsp 26) and heat shock protein Ssa1, which is a ribosome-associated member of

the Hsp70 family participating in the folding of newly-synthesized polypeptides. [60] In addition, the cell division control protein 48 (Cdc48) was less abundant at 9 h.

The results obtained by Wei et al. (2017) on human cancer cells suggest that some ENMs are capable of inducing autophagy and affecting the ER. [61] Schütz et al. (2016) reported that internalized silica nanoparticles (Si-NPs) may accumulate in lysosomes, resulting in lysosomal dysfunction in HeLa cells. [62] Similarly, Si-NPs accumulating in ER indicate an effect on ER structure, through mechanisms still unknown. Any damage to ER is closely connected with cell autophagy, one of the principal cell death mechanisms triggered by ENMs. The acute toxicity of ZnO NPs to Daphnia pulex evidenced by proteomic results showed that some processes such as protein synthesis and translocation across the ER were inhibited to reduce the stress associated to protein misfolding. [63] The majority of the modulated proteins involved in “oxidative phosphorylation” are from the 24 h treatment with CdS QDs, except for the mitochondrial succinate dehydrogenase (ubiquinone) flavoprotein subunit which responded to treatment with CdS QDs at 9 h. Ten of the proteins found in changed amounts after the 24 h treatment with CdS QDs were downregulated suggesting energy production was significantly lessened. These proteins are the mitochondrial succinate dehydrogenase (ubiquinone) iron-sulphur subunit (Sdh2), cytochrome b-c1 complex subunit 6 (Qcr6), the mitochondrial cytochrome b-c1 complex subunit 7 (Qcr7), cytochrome b-c1 complex subunit (Rip1, the Rieske protein), cytochrome c oxidase subunit 4 (Cox4), the mitochondrial cytochrome c oxidase subunit 6 (Cox6), the mitochondrial ATP synthase subunits 5, d, gamma, and delta (Atp5, Atp16, Atp3 and Atp16), while cytochrome c oxidase subunit 2 (Cox2) and the vacuolar isoform of the V-type proton ATPase subunit a (Vph1) were both upregulated. It appears that after 24 h of treatment most of the mitochondrial proteins had reduced activity, causing a slow-down in oxidative phosphorylation and ATP production (Fig. 8). The proteins most affected by the CdS-QDs are components of mitochondrial respiration complexes III, IV and V. Mitochondria are a significant organelle in QD-induced toxicity. [64, 65] It has been shown that CdS QDs damage mitochondrial functionality and reduce respiration activity in yeast, [29] plants, [25] and human cells. [26] Damage to mitochondrial functions and structure caused by several types of metal-ENMs has been found in mollusc bivalve and mouse cells. [66, 67] Interestingly all the proteins of the ATP synthase complex were downregulated, which indicates a reduction in the energy produced through oxidative phosphorylation, and connects with a general downregulation of the enzymes involved in the glycolytic pathway.

In summary, the upregulation of fermentation, but downregulation in the levels of glucose, manifests as a change into lactate or acetate to provide enough energy for survival. These results might bypass the imbalance in the aerobic metabolism and the TCA cycle. Moreover, acetate is also regarded as an expedient source of energy for stressed cells. [68] These observations are consistent with the reports in which silver nanoparticles caused oxidative stress and defects in mitochondrial and endoplasmic reticulum (ER) enzymes. [69, 70] In aerobic metabolism, the formation of ROS is a natural by-product, but an excess of ROS can chemically modify proteins and lipids by lipid peroxidation and oxidative stress, thus leading to damage to vital organelles such as mitochondria, the ER, and lysosomes. [71, 72]

Inhibition of GAPDH activity by CdS QDs

Figure 9 shows that at both 9 and 24 h the activity of GAPDH in yeast cells treated with 100 mg L^{-1} of CdS QDs was significantly lower than in the untreated samples (Fig. 9). Though not highly significant, the activity of GAPDH at 9 h was higher than at 24 h. Overall the CdS QDs treatment at both time points inhibits the glycolytic process at the level of the enzyme GAPDH, as suggested by the proteomic approach (Fig. 6). CdS QD treatment consistently altered GAPDH abundance and decreased GAPDH activity. In vitro experiments in the BY4742 yeast strain on hard corona demonstrated a strong dose-dependent reduction of the enzyme activity upon CdS QDs treatment. [57] The reduction of GAPDH activity by CdS QDs could be explained by CdS QD oxidation of the GAPDH active site (cysteine 152), which is known to lower GAPDH activity and reduce the accessibility to substrates such as glyceraldehyde-3-phosphate. [56, 57] ENPs can induce unfolding and a reduced activity of the identified proteins, as observed in the case of GAPDH isoforms, but CdS QD binding to hard corona proteins could mediate non-specific interactions with other cellular components. [56, 57]

Effect of CdS QDs on ROS generation and cell integrity in S. cerevisiae

Flow cytometry analysis showed that exposure for 9 h to CdS QDs led to a very substantial overproduction of ROS, while significant but much lower ROS overproduction was observed after 24 h of treatment (CdS QDs 100 mg L^{-1}). The results indicate that growth inhibition induced by the treatment was associated with oxidative stress having intense cytotoxic effects at 9 h. Figure 10A and Figure S9 show the time-dependent changes in intracellular production of ROS compared to the untreated control.

Production of ROS by nanomaterials is considered a major factor in QDs toxicity. The deleterious action of oxidative stress starts by causing oxidative damage to biomolecules and destroying their structure, which decreases cellular defences and ultimately leads to cell death, possibly by a mechanism more similar to apoptosis. [73] Overall, our data demonstrate that QDs change the expression levels of a number of proteins by inducing oxidative stress at both treatment periods. Therefore, it is possible to correlate the dysfunction in the glycolysis pathway, the downregulation of oxidative phosphorylation and also the increase in protein misfolding in the ER, all caused by QD treatment, with the production of ROS, which impairs the oxidative balance of the cells and becomes increasingly severe with time. [74, 75]

Figure 10B shows that after 9 h of CdS QDs treatment, the proportion of dead cells was 30% higher with respect to the control, whilst at 24 h the proportion of dead cells increased to 54%. Together these results indicate that cell death increased with the time and dose of CdS QDs. [76, 75]

Robustness of markers identification using multiomic approaches

The proteins that were up or down regulated following CdS QDs treatment were assessed against other omics markers identified using transcriptomics and phenomics, as reported elsewhere analyses. [28, 29, 25] Fig. 11 shows the levels of correlation between proteomics/transcriptomics, phenomics/transcriptomics and proteomics/phenomics markers. These data were obtained by comparing 284 significant proteins against more than 5000 haploid deletion mutants and the whole set of transcripts obtained with a yeast microarray

platform. [28] The correspondences, both symmetric (++/––) and antisymmetric (+-/-+), consisted of a small percentage of the compared elements, i.e. 22 proteins, 14 transcripts, and 8 mutants which responded as were up/ down regulated and/or sensitive/tolerant to the treatment with CdS QDs. It is well known that the correspondence between proteomics and transcriptomics is typically low. [77] The molecular markers that showed this level of correlation in the three comparisons are considered robust enough to be candidates for omics exposure markers. The functions which are most implicated are glycolysis cycle and protein processing in the endoplasmic reticulum. Across the proteins, transcripts and growth phenotypes, the only common element is FKS1, which encodes the catalytic subunit of the yeast 1,3-β-d-glucan synthase, relevant in the building of yeast cell wall and consequently in cell response to materials exposure.

Conclusions

The complexity of biological systems often makes it difficult to study their internal interactions. The choice of S. cerevisiae for this study was informed by the knowledge base for the yeast genetics and omics system, including the characterization of identified entire proteome and genome, the existence of a full set of deletion mutants which cover the entire genome. This approach facilitates the identification of ‘leads’ to be addressed in higher organisms and as models to study human diseases. [34] To explore the mechanism of ENMs toxicity, new approaches utilizing HTS techniques have been advocated. In this study comparative proteomics analysis with 2D-PAGE and iTRAQ revealed some of the final effectors of the responses to CdS QDs in yeast after 9 and 24 h exposure. Key proteins from some of the major metabolic pathways critical to the survival of yeast and other organisms were identified as modulated by the treatment. The most significant Adverse Outcome Pathways (AOPs) influenced by CdS QDs were glycolysis, the oxidative phosphorylation chain, and ubiquitination and trafficking in the endoplasmic reticulum. Some of these AOPs were have also identified been reported in Vietti et al., (2016), and this indicates a need for caution when considering unlimited highlighting the potential adverse effects of an extended use of QDs in the medical field. [78] In addition, it has been demonstrated that CdS QDs generate ROS at both time points, giving rise to increased oxidative damage. These findings will also assist in the establishment of environmental risks associated with the disposal of CdS QD and their interactions with ecosystems, showing how nanobiotechnology can contribute in the safe use of ENMs. [14]

Some of the molecular markers found in this and other studies [28, 29, 25] suggests makes the identification of the markers are reliable and robust. There are few markers in common among proteomics, transcriptomics and phenomics but the recurrence of these within the different tests is significant. As a fact, proteomic markers are “early markers” of cellular exposure, whereas phenomic markers are “global markers” at organismal level. These exposure markers involve systems including mitochondrial function, glycolytic cycle, and ubiquitination in the endoplasmic reticulum, which are among the AOP correlated to human pathologies and identified with the system toxicology approach.

Materials And Methods

Reagents and standards

All reagents and standards were purchased from Sigma-Aldrich (St. Louis, MO, USA) unless otherwise stated.

Synthesis and characterization of the CdS QDs

The synthesis and characterization of water-soluble CdS QDs is reported in “supplementary materials” in Figures S.1. and S.2”. Briefly, from the XRD and HR-TEM it was found that the average static diameter was 5 nm, and the crystal structure was that of hexagonal wurtzite (ZnS) with approximately 78% Cd. Average particle size (dh) of the aggregates (measured with DLS) and zeta potential (ζ) in ddH_2O were estimated as 178.7 nm and + 15.0 mV, respectively; in YPD the values were 545 nm and − 11 mV respectively.

Yeast strains and growth conditions

S. cerevisiae strain BY4742 (MATα his3Δ1 leu2Δ0 lys2Δ0 ura3Δ0) was used in all experiments (79). Cells were grown for 9 and 24 h at 30° with shaking at 130 rpm in a YPD liquid medium (1% w/v yeast extract, 2% w/v peptone, 2% w/v dextrose), without supplementation, or supplemented with 0.25 mg L^{-1} nystatin, or 100 mg L^{-1} CdS QDs, or 0.25 mg L^{-1} nystatin plus 100 mg L^{-1} CdS QDs.

A prior complete analysis of the CdS QDs minimal inhibitory concentration was carried out, using concentrations ranging from 0 to 250 mg L^{-1} (with and without nystatin). [29] Nystatin was added to facilitate the uptake of the CdS QDs. [28] The purity of the cultures was monitored by optical microscopy.

Exposure of yeast cells to different CdS QDs concentrations

Strain BY4742 was grown at 30 °C in YPD medium. After 24 h, optical densities at 600 nm (OD600) were determined using a Cary 50 UV-visible spectrophotometer (Varian, Agilent technologies, TO, Italy), and the OD600 was adjusted to 1.0 with sterile water. The cells were then serially diluted tenfold and aliquots (4 µL) of each dilution were spotted onto 2% w/v SD-agar (6.7 g L^{-1} yeast nitrogen base w/v, glucose 2% w/v, histidine 20 mg L^{-1}, leucine 120 mg L^{-1}, lysine 60 mg L^{-1}, uracil 20 mg L^{-1}) or 2% w/v YPD-agar (yeast extract 1% w/v, peptone 2% w/v, dextrose 2% w/v) in the presence or absence of CdS QDs (25–200 mg L^{-1}). The growth of the cells was monitored after incubation at 30 °C for two days.

To determine the toxicity of the CdS QDs, growth curves were plotted using concentrations ranging from 0 to 200 mg L^{-1} with and without nystatin. Yeast cells were grown starting from liquid cultures pre-grown for about 12 h in YPD until an OD600 of 14 was reached. The cells were subsequently diluted to an OD600 of 0.2 in 10 ml YPD medium supplemented with 25, 50, 100 or 200 mg L^{-1} CdS QDs and cultured at 28 °C under continuous shaking (200 rpm) for 48 h.

Protein extraction and quantification

Cells were sampled after 9 h culture for 2D-gel electrophoresis and at 9 h and 24 h for the iTRAQ experiments. Cell pellets were collected by centrifugation, washed with cold distilled water and stored frozen at -80 °C. For protein extraction for 2D-gel separation, the cells were resuspended in 300 µl of cold denaturing IEF buffer containing 7 M urea, 2 M thiourea, 2% CHAPS, 1% ampholytes (pH 3–10, GE Healthcare), 75 mM DTT (added just before use) containing a protease inhibitor cocktail (Sigma, cat # P8215). [80] For iTRAQ analysis, cells were resuspended in 250 µl extraction buffer containing 7 M urea, 2 M thiourea, 2% CHAPS, 20 mM Tris, and

the protease inhibitor cocktail. Acid-washed glass beads were added in order to mechanically lyse the cells using a Thermo Savant FastPrep® Cell Disrupter (Qbiogene Inc. Carlsbad, CA). The cells were broken by vortexing 4 times for 45 s (the samples were cooled on ice for 30 s between each vortexing step) in the presence of glass beads in a volume equivalent to that of the cell pellet. Glass beads, insoluble material and cell debris were eliminated by centrifugation for 30 min at 4 °C and 12,000 g.

The concentration of proteins in the lysates was determined according to a modified Bradford assay after acidification of the sample buffer with 20 mM HCl. [81] Bovine serum albumin (BSA) was used as a standard. Further sample preparation depended on the subsequent step, i.e. 2D-gel analysis or iTRAQ-labelling.

2D-gel separation and trypsin digestion

For protein separation in the first dimension, 250 µg of each sample was loaded onto 11-cm ReadyStrip pH 4–7 IPG strips (BioRad, USA) which had been rehydrated overnight with 250 µL IEF buffer containing the sample. Proteins were focused using a PROTEAN® i12™ IEF System (BioRad, USA) and by successively applying different voltages to the strip: 250 V (60 min), 1 kV (60 min), and 8 kV (5 h) for a total of 35 kV h^{-1}. After isoelectric focusing, the strips were successively incubated for 15 min in 3 ml of reducing buffer containing 2% w/v DTT, 6 M Urea, 0.375 M Tris-HCl (pH 8.8), 20% w/v glycerol, 2% w/v SDS, and for 15 min in 3 ml alkylating buffer containing 2.5% w/v iodoacetamide, 6 M urea, 0.375 M Tris-HCl (pH 8.8), 2% w/v glycerol. The second dimension (SDS-PAGE) was performed using a CriterionTM Dodeca™ cell (BioRad, USA) and 12% Criterion™ XT Bis-Tris gels (BioRad, USA) in 1 M MOPS (3-(N-morpholino)-propanesulfonic acid) buffer containing 1 M Tris, 20 mM EDTA and 2% w/v SDS. The proteins were stained with QC Colloidal Coomassie G-250 (BioRad, USA) and gel images were recorded using a ChemiDoc™ Imaging System (BioRad, USA). Image analysis was performed using the PDQuest software from BioRad (USA). Three biological replicates were used for each of the four CdS QDS concentrations.

2D-gel images were scanned using the ChemidocMP Imaging System (BioRad) and the images were processed and analysed using the PDQuest v8.0.1 software (BioRad) and checked manually. Spot densities were normalized by local regression and subsequently against the whole gel densities. The relative density of each spot was averaged for three replicate gels and Student's t-test analysis ($p < 0.05$) was performed to determine statistically significant differences in protein abundance. Statistically relevant spots were successively excised from the gels using an EXQuest Spot Cutter (BioRad), destained by soaking the pieces of acrylamide for 30 min in a 1:1 solution of 100 mM ammonium bicarbonate and acetonitrile, and the proteins were hydrolysed with trypsin following the Shevchenko et al. (2006) protocol. [82]

Protein identification

The solutions containing the tryptic peptides were desalted and concentrated to a final volume of 4 µl using a Zip-Tip C18 matrix according to the manufacturer's instructions (Millipore Corporation, Billerica, MA, USA), then dispersed into a α-cyano-4-hydroxycinnamic acid (4-HCCA) matrix prepared by dissolving 4-HCCA in 50% acetonitrile/0.05% trifluoroacetic acid and spotting on a MALDI plate. The samples were subjected to mass spectrometry analysis using a 4800 MALDI-TOF/TOF™ MS analyser (Applied Biosystems, Foster City, CA, USA). Peptide mass spectra were acquired in reflectron mode (500–4000 m/z range) and analysed using the mMass v5.5 open source software (www.mmass.org). For each feature, a peak list was created and manually

checked for the presence of signals from the matrix complex, trypsin and human keratin peptides. The main parameters were set as follows: digestion enzyme, trypsin with one missed cleavage; mass type, monoisotopic; 100 ppm peptide tolerance. Cysteine carbamidomethylation and methionine oxidation were set as fixed and variable modifications, respectively.

Trypsin hydrolysis and iTRAQ labelling

An acetone precipitation was performed to clean each sample by adding six volumes of cold acetone to the solutions containing 100 µg protein and placing the mixtures at − 20 °C for 1 h to allow for the formation of protein precipitates. The resulting precipitates were sedimented by low-speed centrifugation and used for iTRAQ analysis. One hundred µg of proteins from each sample was solubilized in 0.05 M triethylammonium bicarbonate containing 1% sodium deoxycholate. Disulphide bonds were reduced for 1 h at 60 °C in the presence of 5 mM tris (2-carboxyethyl) phosphine, and the resulting free thiol groups were alkylated at room temperature for 15 min using methylmethanethiosulphonate (10 mM). The proteins were hydrolysed for 16 h at 37 °C in the presence of 5% trypsin in 50 mM triethylammonium bicarbonate. The solutions were acidified by the addition of trifluoroacetic acid (TFA) to a final concentration of 0.5% and centrifuged to remove the sodium deoxycholate. The resulting supernatants were transferred to new tubes and dried under vacuum (Qbiogene Inc. Carlsbad, CA). The dried peptides from the yeast samples were dissolved in 100 µl of 250 mM triethylammonium bicarbonate in 75% (v/v) ethanol and transferred to different vials containing the different iTRAQ reagents (114–117; AB SCIEX, Foster City, CA). After 1 h incubation at room temperature, the reactions were stopped by the addition of 100 µl Milli-Q water. The iTRAQ-labelled yeast peptides were pooled, and the mixtures were dried under vacuum. iTRAQ labelling of the peptides from the different biological replicates was performed in the same conditions, except that the labels were inverted to reduce bias between samples.

Strong cation exchange (SCX) fractionation of the iTRAQ-labelled peptides

The dried iTRAQ-labelled peptides were resuspended in 3 ml of sample-loading buffer (10 mM ammonium formate, 20% acetonitrile, pH 3.0) and loaded on a 1-ml NuviaTMS cartridge prepared according to the manufacturer's instructions (BioRad) at 0.5 ml min^{-1} using a syringe pump. After sample loading, the cartridges were washed with 5 ml of sample loading buffer at 0.5 ml min^{-1} and peptide elution was performed at the same flow rate with consecutive 1.5-ml ammonium formate salt plugs at pH 3.0 (30, 50, 80, 100, 125, 150, 175, 200, 225, 250, 275, 300, 325, 350, and 400 mM in 20% acetonitrile). The eluent from each salt plug was dried using a SpeedVac centrifugal vacuum concentrator, and the peptides were purified on a PepClean C-18 column (Thermo Fischer Scientific, USA) prior to MS analysis.

Nano-LC-MS-MS analysis of the strong cation exchange fractions

Peptide analysis was performed by reverse-phase LC–electrospray ionization–MS-MS using a nanoACQUITY Ultra Performance Liquid Chromatography system coupled to a Q-TOF mass spectrometer (Xevo Q-TOF, Waters, Milford, USA). The peptides purified by strong cation exchange chromatography were resuspended in 0.1% TFA and loaded on a C18 trap column (Symmetry 180 µm × 20 mm, 5 µm; Waters, Milford, USA) that was washed with 1% (v/v) acetonitrile and 0.1% (v/v) formic acid at 15 µl min^{-1} for 10 min. The peptides

eluted from the trap column were separated on a C18 analytical column (75 µm × 100 mm, 1.7 µm; Waters, Milford, USA) at 350 nl min^{-1} using 0.1% formic acid as solvent A and 0.1% formic acid in acetonitrile as solvent B in a stepwise gradient: 0.1–10% B (0–10 min), 10–30% B (10–110 min), 30–40% B (110–120 min), 40–85% B (120–125 min), 85% B (125–130 min), and 85–0.1% B (130–135 min). The eluting peptides were sprayed in the mass spectrometer (capillary and cone voltages set to 4 kV and 35 V, respectively), and MS-MS spectra were acquired using automated data-directed switching between the MS and MS-MS modes using the instrument software (MassLynx V4.0 SP4). The five most abundant signals of a survey scan (350–1500 m/z range, 0.9-s scan time) were selected by charge state, and collision energy was applied accordingly for sequential MS-MS fragmentation scanning (50–1800 m/z range, 0.9-s scan time).

Data Processing, protein identification, and quantification

An extensive search was used rigorously to profile the MS data. [83] The MS raw data files were processed using Mascot Distiller (version 2.4.3.2, Matrix Science, London, UK). The resulting “mgf” files were converted into the “.mzXML” file format using msconvert. [84] The “.mzXML” files were searched by MyriMatch version 2.1.120 [85] and X!Tandem version 2011.12.01.1 [86] (LabKey, Insilicos, ISB, Seattle, WA) using the S. cerevisiae protein database and the following settings: trypsin specific digestion with two missed cleavages allowed, peptide tolerance of 100 ppm, fragment tolerance of 0.2 Da, iTRAQ 4-plex for peptide N-t and Lys as fixed modifications, and, in variable mode, iTRAQ 4-plex on Tyr, oxidized Met and methylthio on Cys. For quantitative analysis, all intensities of the iTRAQ reporter ions were extracted using the Trans-Proteomic Pipeline (TPP) tool Libra and the isotopic correction factors from the iTRAQ reagent manufacturer. Normalization of iTRAQ channels was performed by summing all intensities of reporter ions in each iTRAQ channel (for peptides above the Libra probability cut-off) and equalizing each channel contribution by dividing individual reporter ion intensities by the corresponding channel-specific correction factor. All “.pep.xml” files obtained from PeptideProphet were combined using iProphet. [87] A protein list was assembled using ProteinProphet, [88] and the final protein ratios were calculated using Libra. In all searches a concatenated target-decoy database-search strategy was used to check the false positive rate, which was found to be less than 1% in all cases. Peptide sequences were exported for each protein, with a protein and peptide probability cut-off of 0.95. Peptides matching two or more proteins (shared peptides) were excluded from the analysis. Proteins with no unique peptides, i.e. proteins identified by shared peptides only, were also excluded. A protein was considered as identified if it contained at least one unique peptide. Only proteins identified by two or more unique peptides were used for quantification. The method of Ross et al., (2004) was used for statistical analysis of the quantitative data. [89] Briefly, the 115/114, 116/114 and 117/114 ratios corresponding to each protein were calculated for each of the two biological replicates and log2 transformed to obtain a normal distribution. All the values in each comparison dataset were normalized to the median log values, and global means and standard deviations were calculated for each biological replicate. Proteins whose average ratios fell outside a standard deviation of ± 1 from the global mean in at least two of the three biological replicates were considered significantly enriched and chosen for further analysis.

GAPDH activity assay

The activity of GAPDH was determined using a GAPDH Activity Assay Kit (Abcam, Cambridge, England) following the manufacturer’s instructions. The assay is based on spectrophotometric measurement of NADH

formation catalysed by GAPDH. Cultures grown for 9 and 24 h in the presence and absence of 100 mg L^{-1} CdS QDs were diluted to the same OD600 value of 1. Forty-five µl were used for the assay and the reaction was run for 60 min at 37 °C. The absorbance of the reaction mixture was measured at 450 nm in kinetic mode using the iMark™ Microplate Absorbance Reader (Bio-Rad). GAPDH activity (U) was calculated as the amount of NADH produced (nmol) per unit of time (min), and was normalized to the protein content of the whole-cell lysate determined by the Bradford Protein Assay (Bio-Rad Laboratories Inc., Hercules, CA, USA).

Determination of ROS and cell viability by flow cytometry

The peroxide-sensitive fluorescent probe 2',7'-dichlorodihydrofluorescein diacetate (H_2DCFDA; Molecular Probes) was used to assess the generation of intracellular reactive oxygen species (ROS). This compound is converted by intracellular esterases to 2',7'-dichlorodihydrofluorescein, which is then oxidized by intracellular ROS to its highly fluorescent oxidized form (DCF). ROS generation was assessed by incubating yeast for 9 and 24 h with and without 100 mg L^{-1} QDs with 20 µM of H_2DCFDA in the dark. After 30 min incubation, fluorescence was measured with a flow cytometer (NovoCyte; ACEA Biosciences, Inc., San Diego, CA, USA). To distinguish living cells from dead cells a second dye, propidium iodide (PI) (MP Biomedicals, LCC), was utilized. The signal from DCF was detected with a FITC (fluorescein isothiocyanate) band pass filter, and the events (50,000) were determined using the NovoExpress Software (ACEA Biosciences, Inc., San Diego, CA, USA).

Data mining and analysis

All experiments were carried out in triplicate from independent yeast pre-cultures. After checking for normality and variance homogeneity in the dataset, a one-way analysis of variance (ANOVA) was applied, with confidence interval (C.I.) of 95%. Statistical differences between means were deduced using the Bonferroni SHD post hoc test, applying a threshold of $p < 0.005$. SPSS v23 software (http://www.ibm.com/analytics/us/en/technology/spss/) was used for all analyses. Venn diagrams were generated using Venny 2.0 (http://bioinfogp.cnb.csic.es/tools/venny/index.html). Bioinformatics analysis of proteins identified in 2D-gel and iTRAQ was carried out using PANTHER, which is freely available online (http:// www.pantherdb.org/pathway/). For each Gene Ontology (GO) category, Bonferroni correction and a two-tailed Fisher's exact test were used to test the enrichment of the differentially abundant proteins against the whole list of identified proteins. The proteins identified were then subjected to metabolic pathway enrichment analysis, which was conducted according to the instructions from the Kyoto Encyclopaedia of Genes and Genomes (KEGG) Pathway Database.

Abbreviations

2D-SDS PAGE, Two-Dimensional Sodium Dodecyl Sulphate Polyacrylamide Gel Electrophoresis; 3Rs, replace, reduce, and refine (animal testing); 4-HCCA, α-cyano-4-hydroxycinnamic acid; CdS QD, cadmium sulphide Quantum Dot; DCF, dichlorofluorescein; ddH_2O, double-distilled water; dh, hydrodynamic diameter; DLS, Dynamic Light Scattering; DTT, Dithiothreitol; ENMs, Engineered Nanomaterials; GAPDH, glyceraldehyde-3-phosphate dehydrogenase; GO, Gene Ontology; HR-TEM, High-Resolution Transmission Electron Microscopy; HTS, High Throughput Screening; IEF, Isoelectrofocusing; iTRAQ, Isobaric Tag for Relative and Absolute Quantitation; LC-MS, liquid chromatography-mass spectrometry; MALDI-TOF MS, Matrix Assisted Laser

Desorption Ionization-Time of Flight Mass Spectrometry; PI, propidium iodide; ROS, Reactive Oxygen Species; SD medium, synthetic defined medium; SDS, sodium dodecyl sulphate; YPD, yeast extract, peptone, dextrose.

Treatments: “ctr” = non-treated control, “QDs” = treatment with CdS QDs only, “nyst” = treatment with nystatin only, “nystat+QDs” = treatment with CdS QDs in combination with Nystatin.

Declarations

Acknowledgement

We acknowledge: The authors acknowledge the assistance of Gianluca Paredi (Department of Pharmacy, University of Parma) for MS analysis, of CIM (Parma, Italy) for access to MALDI-TOF-MS facilities, of Mirca Lazzaretti (Department of Chemistry, Life Sciences and Environmental Sustainability, University of Parma) for helping with the flow cytometry analysis, and of Luca Pagano (Department of Chemistry, Life Sciences and Environmental Sustainability, University of Parma) for helping with Figure 11. Dr. Martin Shepherd is acknowledged for helpful suggestions and language revision.

Authors’ Contribution

The Author Contribution is as follows: NM, VB, MM organized the experimental setup, collaborated in writing the manuscript. VG and VS performed the experiment, analyzed the data and helped in writing the manuscript. VG and MM designed the figures. ZA and MV synthetized and analyzed the nanomaterials and helped in writing the manuscript.

Funding

The work was funded by the University of Parma under the Doctorate fellowships to VG.

Availability of data and materials

All the data acquired during this research are available from the Corresponding Author after request.

Ethics approval and Consent to Participate

We are not in need of Ethical approval under the Springer guidelines to participate to the manuscript submission.

Consent for publication

All Authors have provided their consent for the manuscript to be published.

Competing Interests

The Authors declare that they do not have competing interests.

Author Detail

Associate Professor Marta marmiroli Ph.D.

Department of Chemistry, Life Science and Environmental Sustainability,

University of Parma,

Parco Area delle Scienze 33/A,

43124 Parma,

Italy.

References

1. Brumfield G. Consumer products leap aboard the nano bandwagon. 2006; 440: 262.
2. Kagan CR, Fernandez LE, Gogotsi Y, Hammond PT, Hersam MC, Nel AE, Penner RM, Willson CG, Weiss PS. Nano Day: celebrating the next decade of Nanoscience and Nanotechnology. ACS Nano. 2016; 10: 9093–9103.
3. McWilliams A. The maturing nanotechnology market: products and applications. Wellesley (MA): BCC Research. 2016.
4. Lai Y, Wang L, Liu Y, Yang G, Tang, C, Deng Y, Li Immunosensors based on nanomaterials for detection of tumor markers. Journal of Biomedical Nanotechnology. 2018; 14:44-65.
5. Reed MA, Randall JN, Aggarwal RJ, Matyi RJ, Moore TM, Wetsel AE. Observation of discrete electronic states in a zero-dimensional semiconductor nanostructure. Rev. Lett., 1988; 60: 535-537.
6. Bruchez M, Moronne M, Gin P, Weiss S, Alivisatos AP. Semiconductor nanocrystals as fluorescent biological labels. Science. 198; 218: 2013-2016.
7. Frecker T, Bailey D, Arzeta-Ferrer X, McBride J, Rosenthal SJ. Review-Quantum Dots and their application in lighting, displays, and biology. Solid. State Technol. 2016; 5: 3019-3031.

8. Jun HK, Careem MA, Arof AK. Quantum dot-sensitized solar cells-perspective and recent developments: a review of Cd chalcogenide quantum dots as sensitizers. Mater. Res. Switz. 2013; 22:148-167.
9. Zhai T, Fang X, Li L, Bando Y, Golberg D. One-dimensional CdS nanostructures: synthesis, properties, and applications. 2010; 2;168–187.
10. Nomura M, Kumagai N, Iwamoto S, Ota Y, Arakawa Y. Laser oscillation in a strongly coupled single-quantum-dot–nanocavity system. Phys. 2010; 6: 279-283.
11. Padmanabhan P, Kumar A, Kumar S, Chaudhary RK, Gulyás B. Nanoparticles in practice for molecular-imaging applications: An overview. Acta Biomater. 2016; 41: 1-16.
12. Benayas A, Ren F, Carrasco E, Marzal V, del Rosal B, Gonfa BA, Juarranz A, Sanz-Rodriguez F, Garcia-Sole DJJ, Ma D. PbS/CdS/ZnS quantum dots: a multifunctional platform for in vivo nearinfrared low-dose fluorescence imaging. Adv. Funct. Mater. 2015; 25:6650–6659.
13. Foda MF, Huang L, Shao F, Han HY. Biocompatible and highly luminescent near-infrared $CuInS_2$/ZnS quantum dots embedded silica beads for cancer cell imaging. ACS Appl. Mater. Interfaces. 2014; 6: 2011-2017.
14. Volkov Y. Quantum dots in nanomedicine: recent trends, advances and unresolved issues. Biophys. Res. Co. 2015; 468; 419-427.
15. Gladkovskaya O, Gunko YK, O'Connor GM, Gogvadze V, Rochev Y. In one harness: the interplay of cellular responses and subsequent cell fate after quantum dot uptake. 2016; 11: 68-81.
16. Bailey RE, Smith AM, Nie S. Quantum dots in biology and medicine. Physica E. 2004; 25:1-12.
17. Tayo LL. Stimuli-responsive nanocarriers for intracellular delivery. Biophys. Rev. 2017; 9: 931–940.
18. Ni X, Jia S, Duan X, Ding D, Li K. Fluorescent nanoparticles for noninvasive stem cell tracking in regenerative medicine. J Biomed Nanotechnol. 2018;14: 240-256.
19. Oliveira WF, Cabrera MP, Santos NRM, Napoleão TH, Paiva PMG, Neves RP, Silva MV, Santos BS, Coelho LCBB, Cabral Filho PE, Fontes A, Correia MTS. Evaluating glucose and mannose profiles in Candida species using quantum dots conjugated with Cramoll lectin as fluorescent nanoprobes. Microbiol Res., 2020; 230:126330. doi: 10.1016/j.micres.2019.126330.
20. Nel AE, Malloy TF. Policy reforms to update chemical safety testing. 2017; 355:1016-1018.
21. Holden PA, Gardea-Torresdey JL, Klaessig F, Turco RF, Mortimer M, Hund-Rinke K, Cohen Hubal EA, Avery D, Barceló D, Behra R, Cohen Y, Deydier-Stephan L, *et al*. Considerations of environmentally relevant test conditions for improved evaluation of ecological hazards of engineered nanomaterials. Environ. Sci. Technol. 2016; 50:6124–6145.
22. Derfus AM, Chan WCW, Bhatia, SN. Probing the cytotoxicity of semiconductor Quantum Dots. Nano Lett. 2004; 4: 11-18.
23. Marmiroli M, Pagano L, Savo Sardaro ML, Villani M, Marmiroli N. Genome-wide approach in Arabidopsis thaliana to assess the toxicity of cadmium sulfide quantum dots. Sci. Technol. 2014; 48: 5902–5909.
24. Oh E, Liu R, Nel A, Boeneman Gemill K, Bilal M, Cohen Y, Medintz IL. Meta-analysis of cellular toxicity for cadmium containing quantum dots. Nanotech. 2016;11: 479-4812.
25. Pagano L, Caldara M, Villani M, Zappettini A, Marmiroli N, Marmiroli M. In vivo-in vitro comparative toxicology of cadmium sulphide quantum dots in the model organism *Saccharomyces cerevisiae*.

Nanomaterials. 2019; 9: 512-529.

26. Paesano L, Perotti A, Buschini A, Carubbi C, Marmiroli M, Maestri E, Iannotta S, Marmiroli N. Markers for toxicity to HepG2 exposed to cadmium sulphide quantum dots; damage to mitochondria. Toxicology. 2016; 374: 18–28.
27. Majumdar S, Ma C, Villani M, Zuverza-Mena, N, Pagano L, Huangb Y, Zappettini A, Keller AA, Marmiroli N, Parkash Dhankher O, White JC. Surface coating determines the response of soybean plants to cadmium sulfide quantum dots. 2019; 14:100-151.
28. Marmiroli M, Pagano L, Pasquali F, Zappettini A, Tosato V, Bruschi CV, Marmiroli N. A genome-wide nanotoxicology screen of Saccharomyces cerevisiae mutants reveals the basis for cadmium sulphidequantum dot tolerance and sensitivity. 2016; 10:84–93.
29. Pasquali F, Agrimonti C, Pagano L, Zappettini A, Villani M, Marmiroli M, White J. C, Marmiroli N. Nucleo-mitochondrial interaction of yeast in response to cadmium sulfide quantum dot exposure. J. Hazard. Mater. 2017; 324: 744–752.
30. Zhang T, Hu Y, Tang M, Kong L, Ying J, Wu T, Xue Y, Pu Liver toxicity of cadmium telluride quantum dots (CdTe QDs) due to oxidative stress in vitroand in vivo. Int. J. Mol. Sci. 2015; 16(10): 23279-23299.
31. Fan J, Sun Y, Wang S, Li Y, Zeng X, Cao Z, Yang P, Song P, Wang Z, Xian Z, Gao H, Chen Q, Cui D, Ju D. Inhibition of autophagy overcomes the nanotoxicity elicited by cadmium-based quantum dots. 2016; 78:102–114.
32. Dos Santos SC, Sá-Correia I. Yeast toxicogenomics: lessons from a eukaryotic cell model and cell factory. Opin. Biotechnol. 2015; 33: 183-191.
33. Burden N,Aschberger K, Chaudhry Q, Clift MJD, Doak SH, Fowler P, Johnston H, Landsiedel R, Rowland J, Sone V. The 3Rs as a framework to support a 21st century approach for nanosafety assessment. Nano Today. 2017; 12:10-13.
34. Zhang T, Gaffrey M J, Thrall BD, Qian WJ. Mass spectrometry-based proteomics for system-level characterization of biological responses to engineered nanomaterials. Bioana Chem. 2018; 410: 6067–6077.
35. Scala G, Kinareta P, Marwah V, Sund J, Fortino V, Greco D. Multi-omics analysis of ten carbon nanomaterials effects highlights cell type specific patterns of molecular regulation and adaptation. 2018;11: 99–108.
36. Duina AA, Miller ME, Keeney JB. Budding yeast for budding geneticists: a primer on the Saccharomyces cerevisiae model system. Genetics. 2014; 197:33–48.
37. Griffin TJ, Gygi SP, Ideker T, Rist B, Eng J, Hood L, Aebersold Complementary profiling of gene expression at the transcriptome and proteome levels in *Saccharomyces cerevisiae*. Molecular & Cellular Proteomics. 2002; 1(4): 323-333.
38. Goffeau A. Four years of post-genomic life with 6000 yeast genes. FEBS Lett. 2000; 480:37- 41.
39. Hillenmeyer ME, Fung E, Wildenhain J, Pierce SE, Hoon S, Lee W, Proctor M, St.Onge RP, Tyers M, Koller D, Altman RB, Davis RW, Nislow C, Giaever G. The chemical genomic portrait of yeast: uncovering a phenotype for all genes. 2008; 320:362–365.

40. Bao S, Lu Q, Fang T, Dai H, Zhang C. Assessment of the toxicity of CuO nanoparticles by using *Saccharomyces cerevisiae* mutants with multiple genes deleted. Environ. Microbiol. 2015; 81: 8098–8107.
41. Dos Santos SC, Teixeira MC, Cabrito T R, Sá-Correia I. Yeast toxicogenomics: genome-wide responses to chemical stresses with impact in environmental health, pharmacology, and biotechnology. Genet. 2012; 3:63.
42. Campanerut-Sá PAZ, Ghiraldi-Lopes, LD, Meneguello JE, Teixeira JJV, Scodro RBDL, Siqueira VLD, Svidzinski TIE, Pavan FR, Cardoso RF. Systematic review on the proteomic profile of Mycobacterium tuberculosis exposed to drugs. Clin. App. 2017; 11: 11-12.
43. Kerry RG, Mahapatra GP, Patra S, Sahoo SL, Pradhan C, Padhi BK, Rout JR. Proteomic and genomic responses of plants to nutritional stress. BioMetals. 2018; 31: 161-187.
44. Pavelka N, Rancati G, Zhu J, Bradford WD, Saraf A, Florens L, Sanderson BW, Hattem GL, Li R. Aneuploidy confers quantitative proteome changes and phenotypic variation in budding yeast. 2010; 468: 321-325.
45. Insensera MR, Hernáezb ML, Nombelaa C, Molina M, Moleroa G, Gila C. Gel and gel-free proteomics to identify Saccharomyces cerevisiae cell surface proteins. J. Proteomics. 2010; 73: 1183-1195.
46. Nightingale DJH, Geladaki A, Breckels LM, Oliver SG, Lilley KS. The subcellular organisation of *Saccharomyces cerevisiae.* Opin. Cell. Biol. 2019; 48: 86–95.
47. Tafelmeyer P, Laurent C, Lenormand P, Rousselle J-C, Marsollier L, Reysset G, Zhang R, Sickmann A, Stinear TP, Namane A, Cole ST. Comprehensive proteome analysis of Mycobacterium ulceransand quantitative comparison of mycolactone biosynthesis. 2008; 8:3124-3138.
48. Radosevich TJ, Reinhardt TA, Lippolis JD, Bannantine JP, Stabel JR. Proteome and differential expression analysis of membrane and cytosolic proteins from *Mycobacterium avium subsp. paratuberculosis* strains K-10 and 187. J. Bacteriol. 2007;189: 1109–1117.
49. Pütz SM, Boehm AM, Stiewe T, Sickmann A. iTRAQ Analysis of a Cell Culture Model for Malignant Transformation, Including Comparison with 2D-PAGE and SILAC. *J.* Proteome Res. 2012; 11:2140–2153.
50. Lee YJ, Jang JW, Kim KJ, Maeng PJ. TCA cycle-independent acetate metabolism via the glyoxylate cycle in Saccharomyces cerevisiae. 2011; 28:153–166.
51. Kaplan RS, Mayor JA, Kakhniashvili D, Gremse DA, Wood DO, Nelson DR. Deletion of the nuclear gene encoding the mitochondrial citrate transport protein from *Saccharomyces cerevisiae*. Biochem. Biophys. Res. Commun. 1996.226, 657–662.
52. Peng Q, Huo D, Li H, Zhang B, Li Y, Liang A, Wang H, Yu Q, Li M. ROS-independent toxicity of Fe_3O_4nanoparticles to yeast cells: involvement of mitochondrial dysfunction. Biol. Interact. 2018; 287: 20-26.
53. Sousa CA, Soares HVM, Soares EV. Nickel Oxide (NiO) Nanoparticles induce loss of cell viability in yeast mediated by oxidative stress. Res. Toxicol. 2018; 31:658–665.
54. Gomes A, Sengupta J, Datta P, Ghosh S, Gomes A. Physiological interactions of nanoparticles in energy metabolism, immune function and their biosafety: a review, J Nanosci. and Nanotech. 2016; 16:92–116.
55. Horstmann C, Kim DS, Campbell C, Kim K. Transcriptome Profile Alteration with Cadmium Selenide/Zinc Sulfide Quantum Dots in *Saccharomyces cerevisiae.* 2019; 9(11) E653. doi: 10.3390/biom9110653.

56. Ghosh S, Ray M, Das MR, Chakrabarti A, Khan AH, Sarma DD, Acharya Modulation of glyceraldehyde-3-phosphate dehydrogenase activity by surface functionalized quantum dots. Phys. Chem. Chem. Phys. 2014; 16: 5276-5283.
57. Ruotolo R, Pira G, Villani M, Zappettini A. Marmiroli N. Ring-shaped corona proteins influence the toxicity of engineered nanoparticles to yeast. **Sci. Nano.** 2018; **5**: 1428-1440.
58. Franzosa EA, Albanese V, Frydman J, Xia Y, McClellan AJ. Heterozygous yeast deletion collection screens reveal essential targets of Hsp90. PloS one. 2011; 6: e28211.
59. Sundarraj K, Raghunath A, Panneerselvam L, Perumal E. Iron oxide nanoparticles modulate heat shock proteins and organ specific markers expression in mice male accessory organs. Tox Appl. Pharmacol. 2017; 317: 12-24.
60. Willmund F, del Alamo M, Pechmann S, Chen T, Albanese V, Dammer The cotranslational function of ribosome-associated Hsp70 in eukaryotic protein homeostasis. Cell. 2013;152: 196-209.
61. Wei F, Wang Y, Zewei LZ, Li Y, Duan Y. New findings of silica nanoparticles induced ER autophagy in human colon cancer cell. Sci. Rep. 2017; 7:42591.
62. Schütz I, Lopez-Hernandez T, Gao Q, Puchkov D, Jabs S, Nordmeyer D, Schmudde M, Rühl E, Graf CM, Haucke V. Lysosomal dysfunction caused by cellular accumulation of silica nanoparticles. J Biol. Chem. 2016; 291:14170-14184.
63. Lin L, Xu M, Mu H, Wang W, Sun J, He J, Qiu JW, Luan T. Quantitative proteomic analysis to understand the mechanisms of Zinc Oxide Nanoparticle toxicity to *Daphnia pulex* (Crustacea: Daphniidae): Comparing with Bulk Zinc Oxide and Zinc Salt. Sci. Technol. 2019; 7:5436-5444.
64. Cho SJ, Maysinger D, Jain M, Roder B, Hackbarth S, Winnik FM. Long-term exposure to CdTe quantum dots causes functional impairments in live cells. Langmuir. 2007; 23 (4):1974–1980.
65. Katubi KM, Alzahrani FM, Ali D, Alarifi S. Dose- and duration-dependent cytotoxicity and genotoxicity in human hepato carcinoma cells due to CdTe QDs exposure. Exp. Toxicol. 2019; 38(8): 914-926. doi: 10.1177/0960327119843578.
66. Lopes Rocha T, Gomes T, Serrão Sousa Nélia, V, Mestre C, João Bebianno M. Ecotoxicological impact of engineered nanomaterials in bivalve molluscs: An overview. Environ. Res. 2015; 111: 74-88.
67. PereiraLC, Pazin M, Franco-Bernardes MF, Martins ADC, Barcelos GRM, Pereira MC, Mesquita JP, Rodrigues JL, Barbosa F, Dorta A perspective of mitochondrial dysfunction in rats treated with silver and titanium nanoparticles (AgNPs and TiNPs). J. Trace Elem. Med. Biol. 2018; 47: 63-69.
68. Jiang L, Gulanski BI, De Feyter HM, Weinzimer SA, Pittman B, Guidone E, *et al.* Increased brain uptake and oxidation of acetate in heavy drinkers, J. Clin. Investig., 2013; 123 (4):1605–1614.
69. Teodoro JS, Simões AM, Duarte FV, Rolo AP, Murdoch RC, Hussain SM, *et al*. Assessment of the toxicity of silver nanoparticles in vitro: a mitochondrial perspective. Toxicol. Vitro. 2011; 25 (3): 664–670.
70. Jarak I, Carrola J, Barros AS, Gil AM, Pereira ML, Corvo ML, *et al*. From the cover: metabolism modulation in different organs by silver nanoparticles: an NMR metabolomics study of a mouse model, Toxicol. , 2017;159 (2): 422–435.
71. McShan D, Ray PC, Yu H. Molecular toxicity mechanism of nanosilver. J. Food Drug Anal. 2014: 22 (1): 116–127.

72. Márquez IG, Ghiyasvand M, Massarsky A, Babu M, Samanfar B, Omidi K, *et al.* Zinc oxide and silver nanoparticles toxicity in the baker's yeast, Saccharomyces cerevisiae. PloS One. 2018. 13 (3): e0193111. 10.1371/journal.pone.0193111
73. Ipe BI, Lehnig M, Niemeyer CM. On the generation of free radical species from quantum dots. 2005; 1:706-709.
74. Chen S, Ren Q, Zhang J, Ye Y, Zhang Z, Xu Y, Guo M, Ji H, Xu C, Gu C, Gao W, Huang S, Chen N-acetyl-L-cysteine protects against cadmium-induced neuronal apoptosis by inhibiting ROS-dependent activation of Akt/mTOR pathway in mouse brain. Neuropath. Appl. Neuro. 2014; 40: 759-777.
75. Han PP, Shen SG, Guo RJ, Zhao DX, Lin YH, Jia SR, Yan RR, Wu YK. ROS is a factor regulating the increased polysaccharide production by light quality in the edible *Cyanobacterium Nostoc flagelliforme*. Agric. Food Chem. 2018; 67:2235-2244.
76. Qu Y, Li W, Zhou Y, Liu X, Zhang L, Wang L, Li YF, Iida A, Tang Z, Zhao Y, Chai Z, Chen C. Full assessment of fate and physiological behavior of Quantum Dots utilizing *Caenorhabditis elegans* as a model organism. Nano Lett.2011; 11:3174–3183.
77. Marmiroli M, Imperiale D, Pagano L, Villani M, Zappettini A, Marmiroli N. The Proteomic Response of Arabidopsis thaliana to Cadmium Sulfide Quantum Dots, and Its Correlation with the Transcriptomic Response. Front Plant Sci. 2015; 16; 6:1104.
78. Vietti G, Lison D, van der Brule S. Mechanisms of lung fibrosis induced by carbon nanotubes: towards an Adverse Outcome Pathway (AOP). Part Fibre Toxicol. 2015; 13:11.
79. Giaever G, Nislow C. The yeast deletion collection: a decade of functional genomics. 2014; 197: 451–465.
80. Slibinskas R, Ražanskas R, Zinkevičiūtė R, Čiplys E. Comparison of first dimension IPG and NEPHGE techniques in two-dimensional gel electrophoresis experiment with cytosolic unfolded protein response in Saccharomyces cerevisiae. Proteome Sci. 2013; 11: 2736-42.
81. Ramagli LS, Rodriguez LV. Quantitation of microgram amounts of protein in SDS -mercaptoethanol-tris electrophoresis sample buffer. Electrophoresis. 1985; 6: 559–563.
82. Shevchenko A, Tomas H, Havlis J, Olsen JV, Mann M. In-gel digestion for mass spectrometric characterization of proteins and proteomes. Protoc. 2006; 1: 2856– 68760.
83. Srivastava V, Malm E, Sundqvist G, Bulone V. Quantitative proteomics reveals that plasma membrane microdomains from poplar cell suspension cultures are enriched in markers of signal transduction, molecular transport, and callose biosynthesis. Cell Proteomics. 2013;12: 3874-3885.
84. Kessner D, Chambers M, Burke R, Agus D, Mallick P. ProteoWizard: open source software for rapid proteomics tools development. 2008; 24: 2534–2536.
85. Tabb DL, Fernando CG, Chambers MC. MyriMatch: highly accurate tandem mass spectral peptide identification by multivariate hypergeometric analysis. J. Proteome Res. 2007; 8:654–661.
86. Craig R, Beavis RC. TANDEM: matching proteins with mass spectra. 2004; 20: 1466–1467.
87. Shteynberg D, Deutsch EW, Lam H, Eng JK, Sun Z, Tasman N, Mendoza L, Moritz RL, Aebersold R, Nesvizhskii AI. iProphet: multi-level integrative analysis of shotgun proteomic data improves peptide and protein identification rates and error estimates. Cell. Proteomics. 2011; 10: 12, M111.007690.

88. Nesvizhskii AI, Keller A, Kolker E. Aebersold. ProteinProphet: a statistical model for identifying proteins by tandem mass spectrometry. Chem. 2003; 75: 4646–4658.
89. Ross PL, Huang YN, Marchese J, Williamson B, Parker K, Hattan S, Khainovski N, Pillai S, Dey S, Daniels S, Purkayastha S, Juhasz P, Martin S, Bartlet-Jones M, He F, Jacobson A, Pappin D. Multiplexed protein quantitation in *Saccharomyces cerevisiae* using amine-reactive isobaric tagging reagents. Cell. Proteomics. 2004; 3:1154–1169.

Supplementary Information

Additional file 1:

Nanoparticles characterization

Figure S1. HRTEM image of ligand-free QDs assembly and X-ray diffraction pattern

Figure S2. (A) ESEM image of the CdS QDs agglomerates. (B) X ray spectra corresponding to the red rectangle in figure S2A.

Figure S3. 2D-gel electrophoresis for the 9 h treatments.

Figure S4. Venn diagram showing the number of unique proteins identified and quantified from the iTRAQ analysis of two biological replicates (BR1 and BR2) for the 9 h treatment corresponding to the four developmental stages.

Figure S5. Venn diagram showing the number of unique proteins identified and quantified from the iTRAQ analysis of two biological replicates (BR1 and BR2) for the 24 h treatment corresponding to the four developmental stages.

Figure S6. Comparison of the number of proteins isolated and identified with iTRAQ and 2D-PAGE for the 9 h treatment. The Venn diagram (A) depicts the numbers of isolated proteins. The Venn diagram (B) depicts the numbers of significantly modulated proteins.

Figure S7. Proteins differentially regulated in the four conditions.

Figure S8. Gene Ontology slim, enrichment analyses

Figure S9. Flow cytometry measurements. Yeast were stained with DCFHDA and PI and detected by flow cytometry after 30 min incubation in the dark. The lateral axis represents the fluorescence of DCFH while vertical axis indicates PI intensity of detected cells.

Table S4: Description of the differentially abundant proteins at 9 h with 2d-gel (A), 9 h with iTRAQ (B), and 24 h with iTRAQ (C).

Additional file 2:

Table S1: MALDI-TOF/TOF data associated with differentially abundant proteins identified by 2d-gel at 9 h.

Table S2: List of all unique proteins, identified by iTRAQ experiments at 9 h from the two biological replicate.

Table S3: List of all unique proteins, identified by iTRAQ experiments at 24 h from the two biological replicate.

Supplementary Tables B1, B2 and B3 are reported in excel format.

Figures

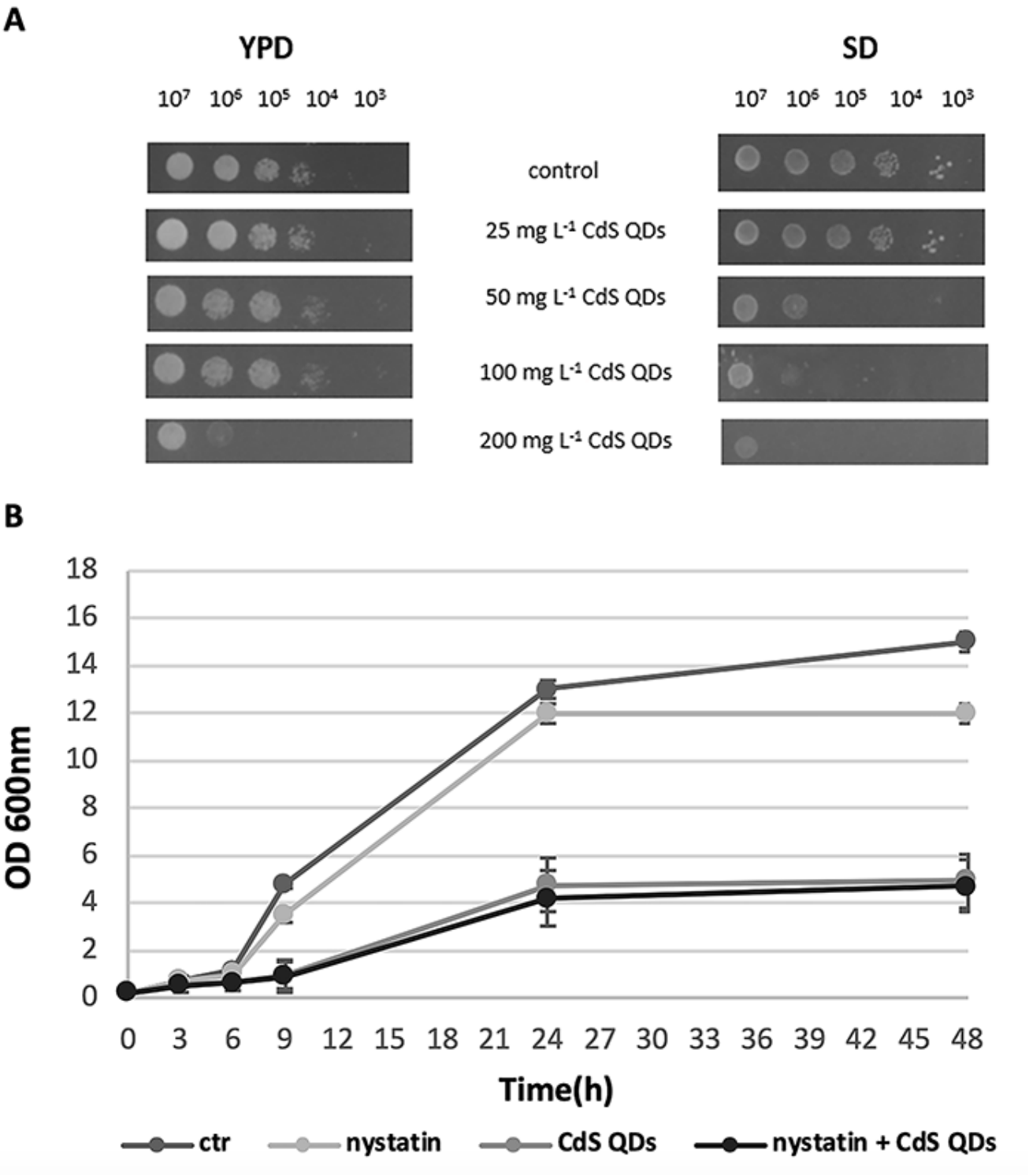

Figure 1

Spot assay and growth curve of S. cerevisiae cells. BY4742 grown on different media: YPD and SD. A) growth at different cell dilutions as affected by the treatment conditions: control, 25, 50, 100, 200 mg L-1. Cells concentrations, used for the different tests, are indicated in the first row of the panel. B) Growth curve of BY4742 with and without nystatin at 100 mgL-1 CdS QDs for 48 hours.

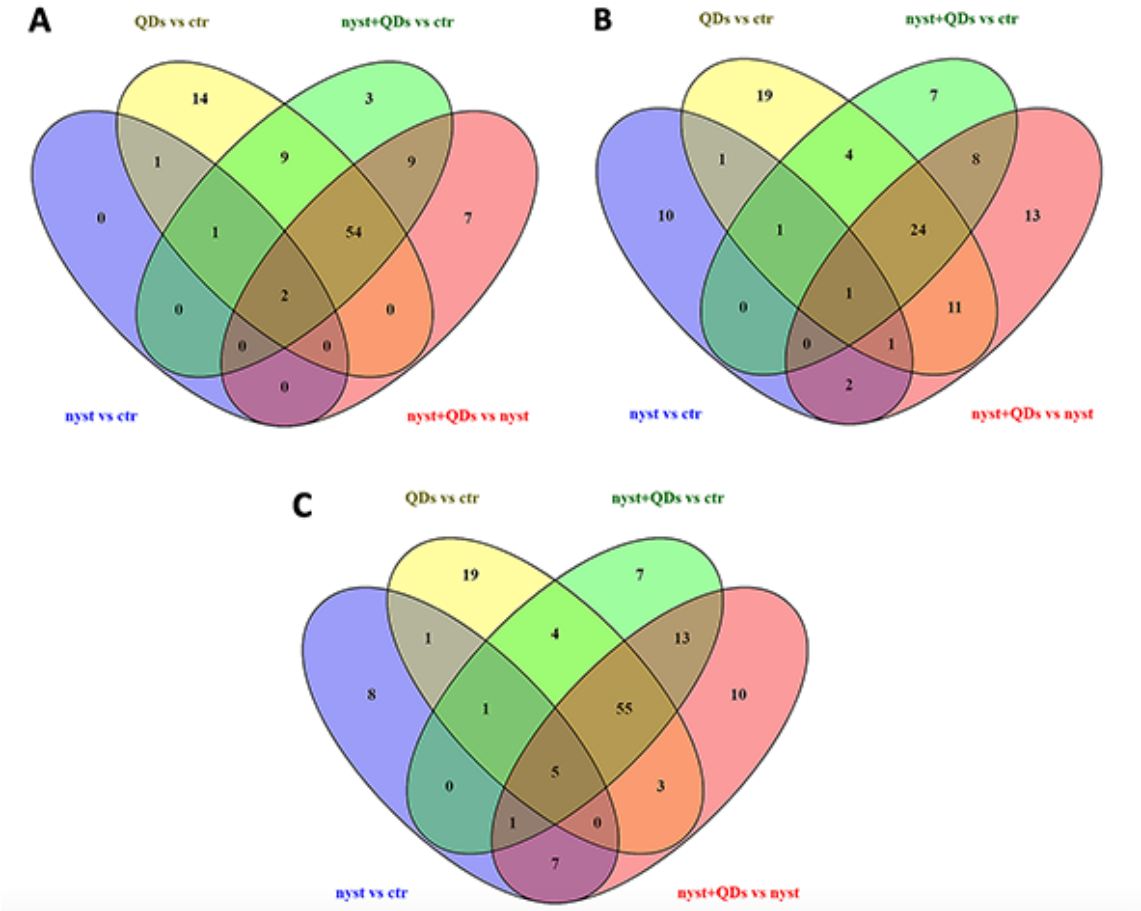

Figure 2

Venn diagrams for the differentially regulate proteins in all treatment conditions. A) 9 h iTRAQ; B) 9 h 2D-gel electrophoresis; C) 24 h iTRAQ.

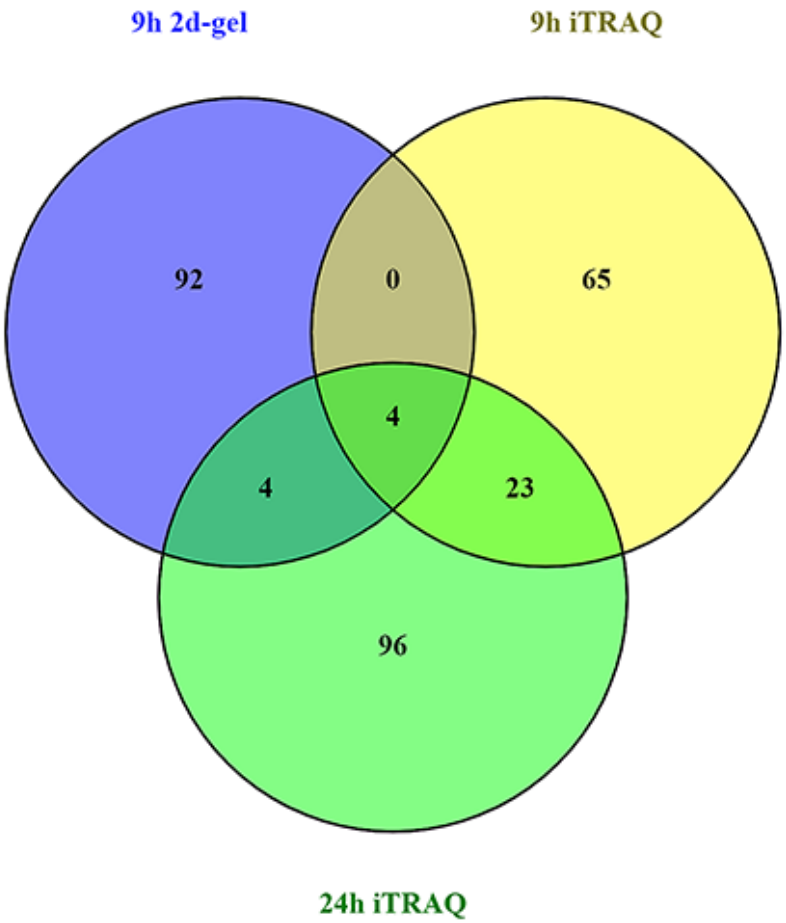

Figure 3

Venn diagram comparing the number of proteins significantly modulated in 2D-gels (9 h treatment), and after iTRAQ analysis (9 and 24 h treatments).

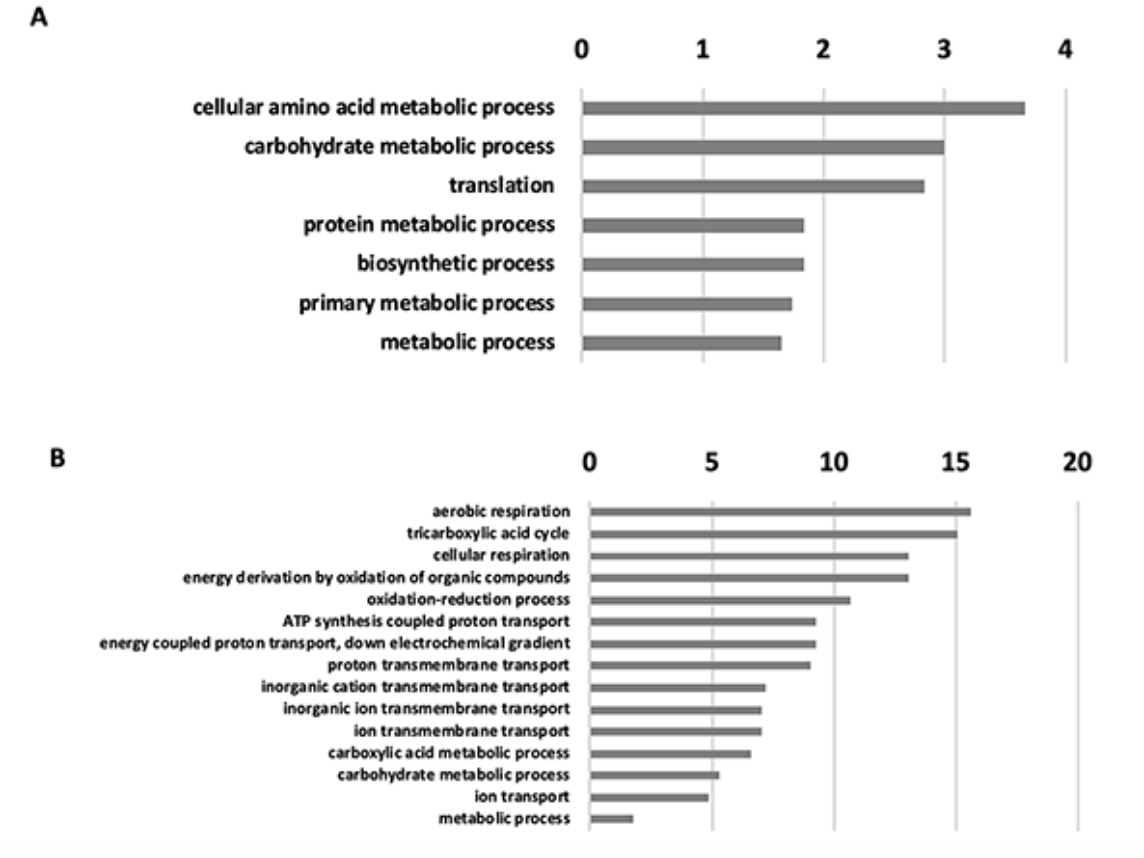

Figure 4

Gene Ontology and enrichment analyses with fold enrichment = -log10 (Fisher's exact p value) for Biological processes: A) 9 h; B) 24 h

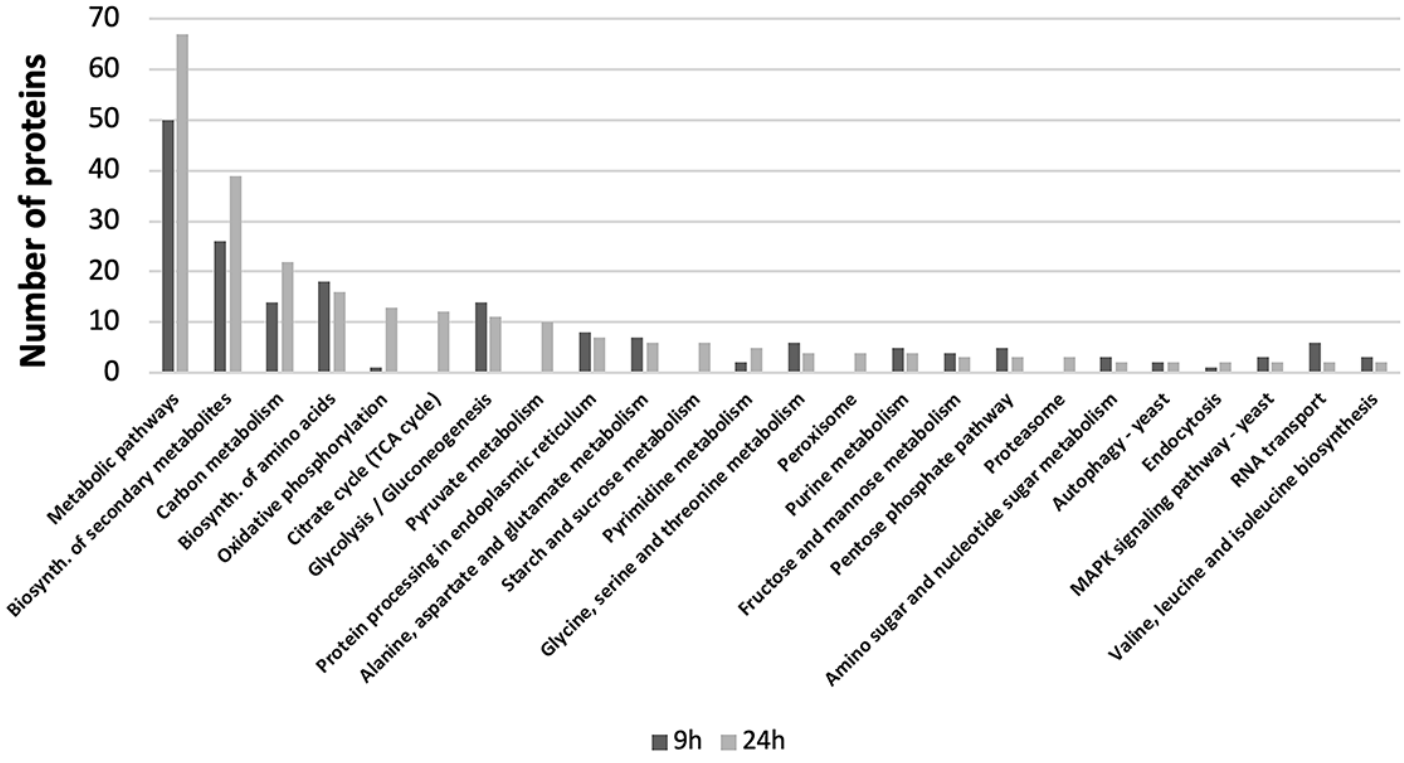

Figure 5

Pathway analysis: Distribution of responsive proteins in yeast at 9 and 24 h, according to the KEGG pathway classification. Black bars are for the proteins found in the 9 h treatment, grey bars represent the proteins found in the 24 h treatment.

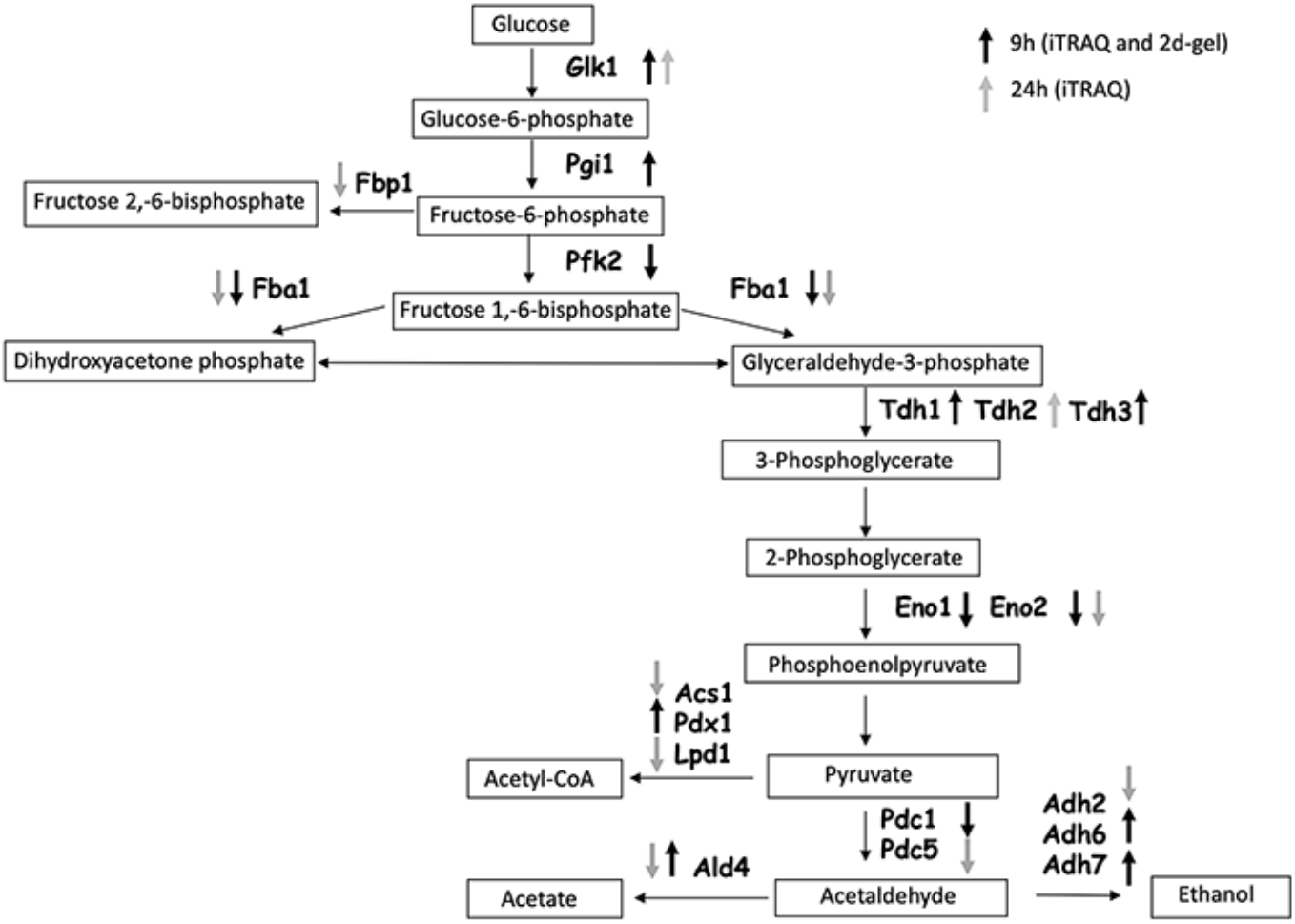

Figure 6

Glycolysis and gluconeogenesis pathway. Black arrows are for the proteins found after 9 h treatment, grey arrows are for the proteins found after 24 h treatment. Arrows pointing up indicate upregulated proteins, arrows pointing down indicate downregulated proteins.

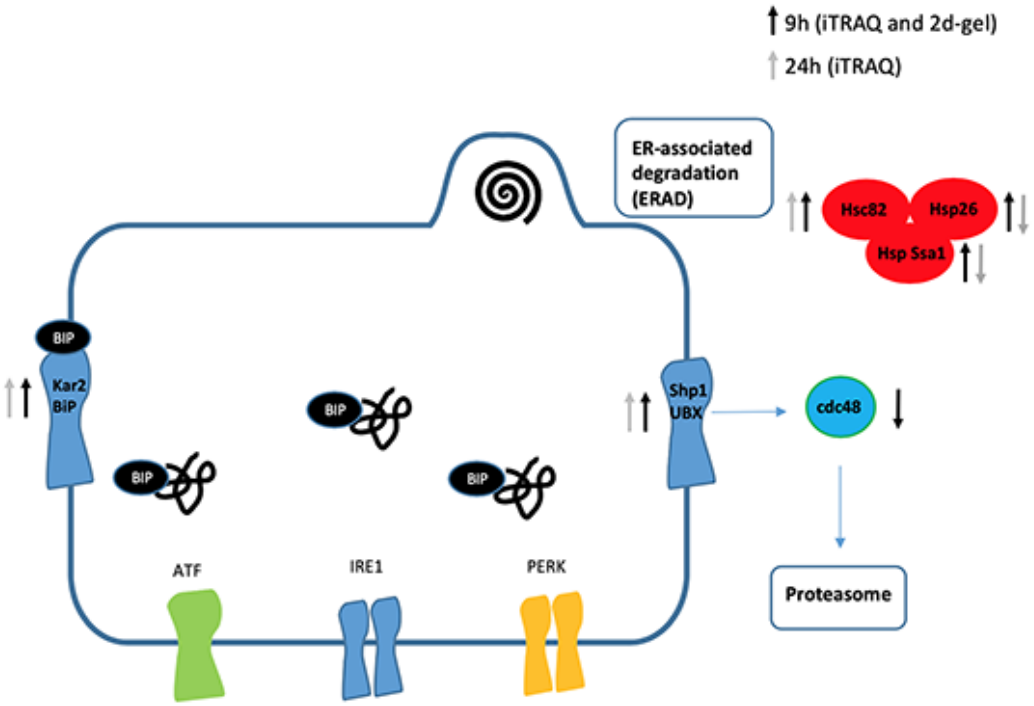

Figure 7

Protein processing in the Endoplasmic Reticulum (ER) pathway. Black arrows are for the proteins found after 9 h treatment, grey arrows are for the proteins found after 24 h treatment. Arrows pointing up indicate upregulated proteins, arrows pointing down indicate downregulated proteins.

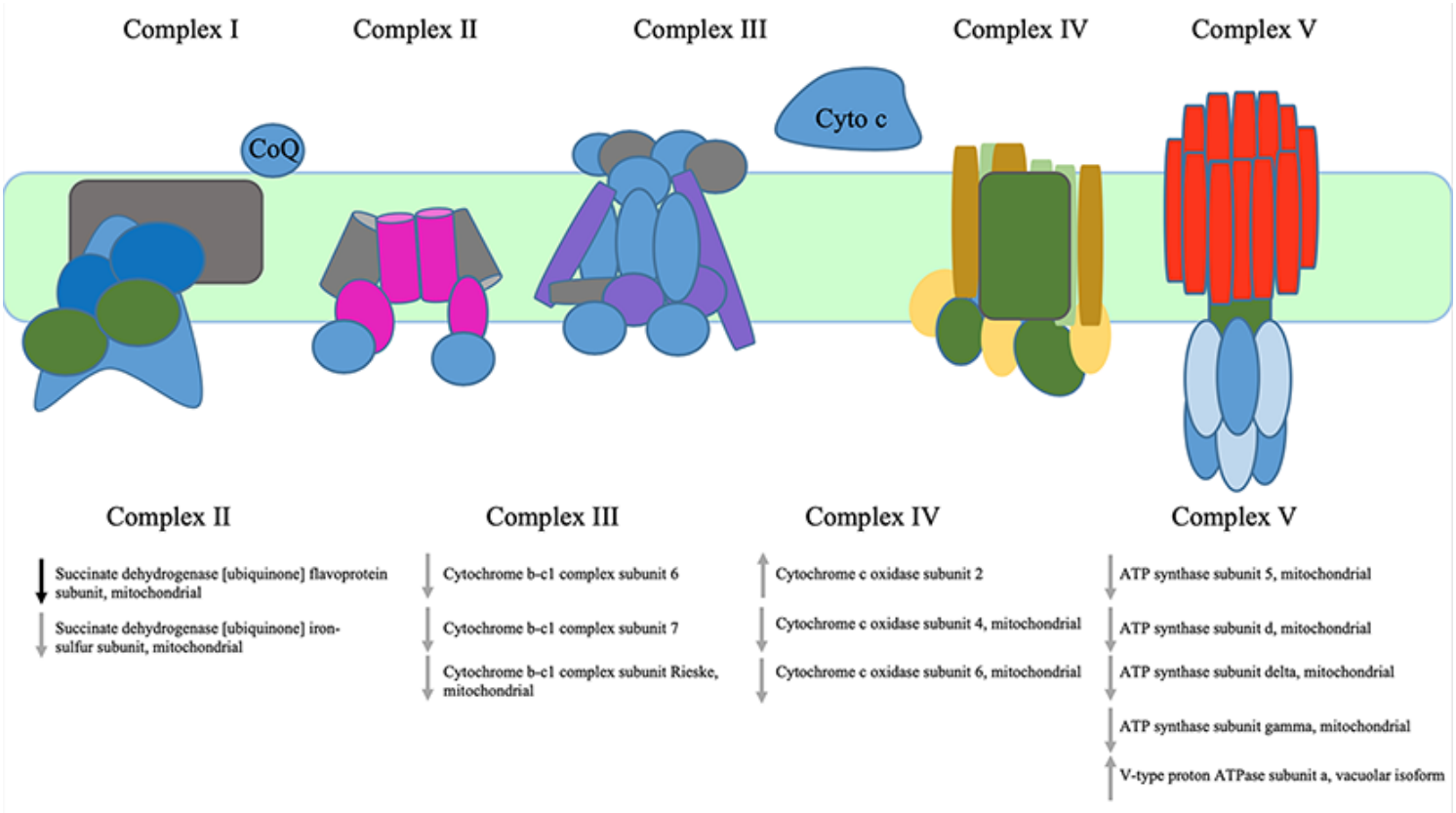

Figure 8

Oxidative phosphorylation pathway. Black arrows are for the proteins found after 9 h treatment, grey arrows are for the proteins found after 24 h treatment. Arrows pointing up indicate upregulated proteins, arrows pointing down indicate downregulated proteins.

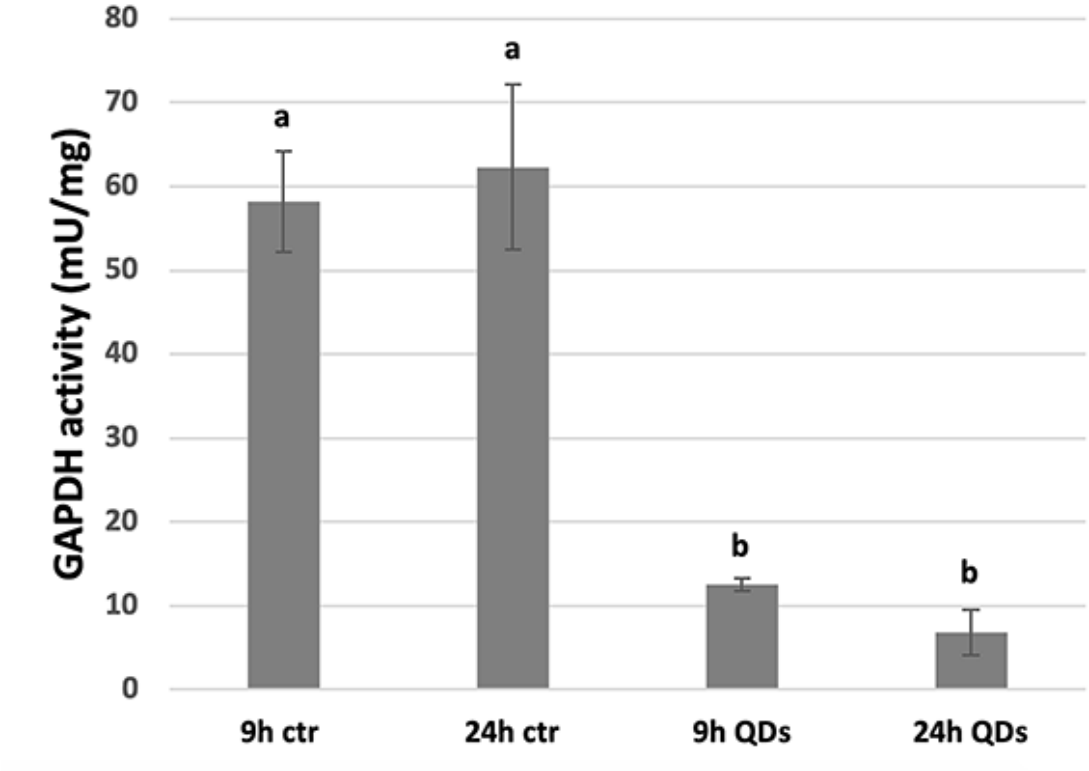

Figure 9

GAPDH (glyceraldehyde-3-phosphate dehydrogenase) activity. ANOVA average of three replicates followed by Bonferroni post hoc test. Different letters indicate a statistic difference with $p < 0.001$.

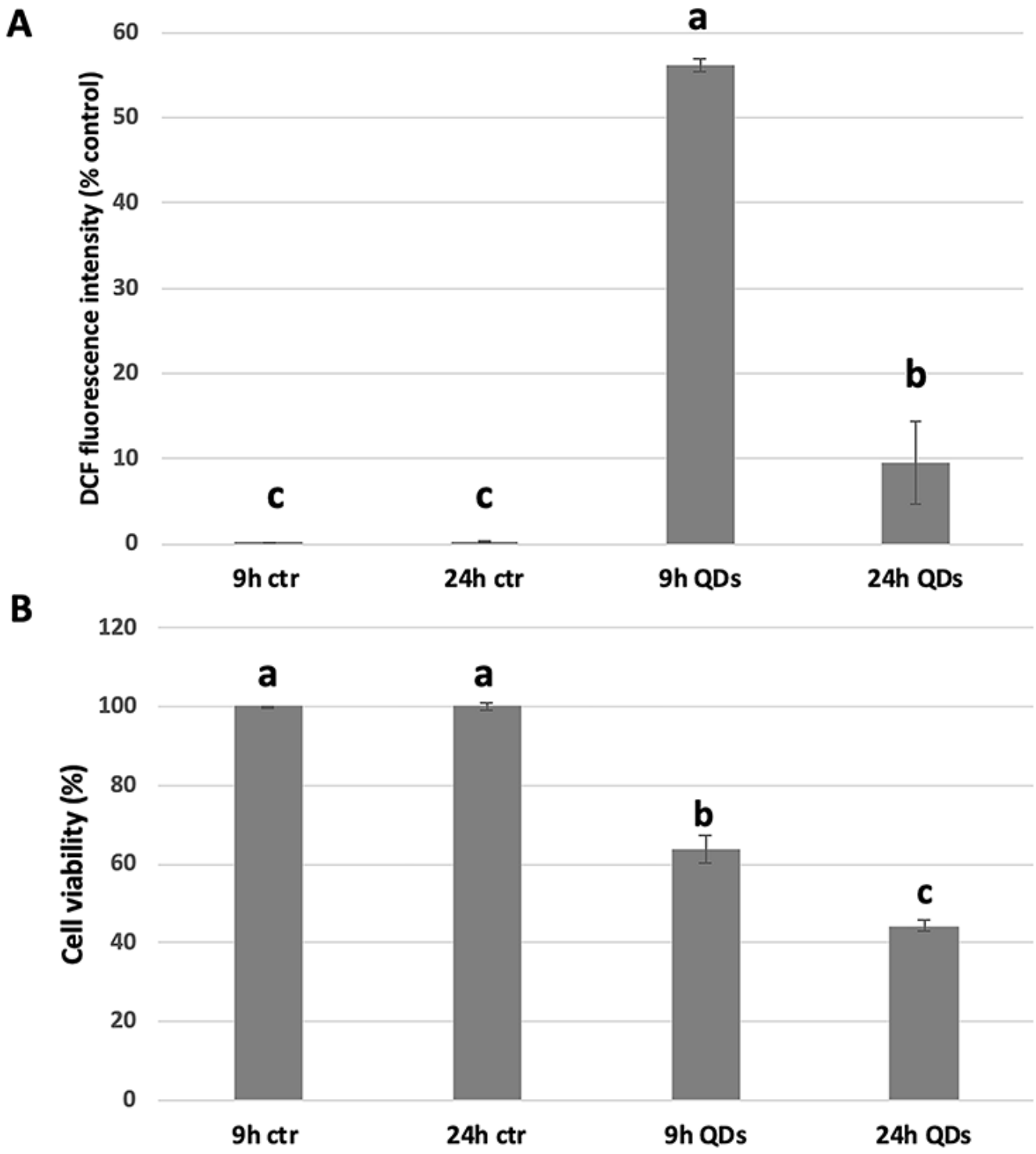

Figure 10

Flow cytometric measurements. The bars represent the average of 4 independent replicates. ANOVA was carried out followed by Bonferroni post hoc test. Different letters indicate a statistic difference with $p < 0.001$: A) changes in intracellular ROS; B) Cell viability evaluated by flow cytometry with propidium iodide.

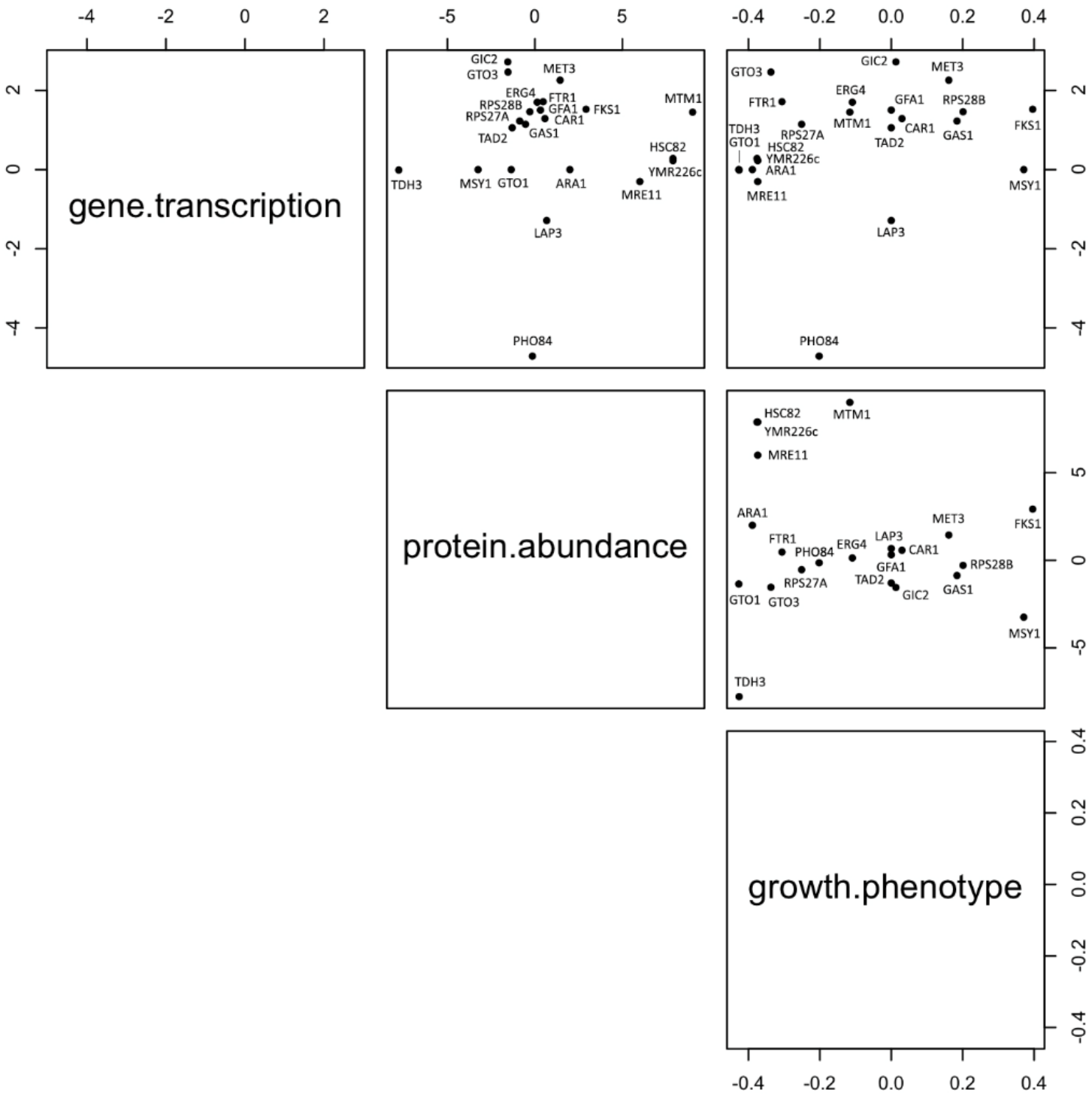

Figure 11

Scatterplot matrix of the independent variables: transcriptome, proteome, and phenome. Three dimensional scatterplot representing the correlation among gene expression, protein abundance and growth phenotype. Phenomics data are taken from Marmiroli et al., 2016, transcrptomics data from Pagano et al., 2019.

Supplementary Files

This is a list of supplementary files associated with this preprint. Click to download.

- Additionalfile2SMS1S3.xlsx
- Additionalfile1supplementarymaterial.docx